Research Square

Preprints are preliminary reports that have not undergone peer review.
They should not be considered conclusive, used to inform clinical practice,
or referenced by the media as validated information.

A Novel Kokumi Peptide RSQPVGV from Yeast Extract via CaSR-Mediated Taste Enhancement

Haofeng Lao
Shanghai Institute of Technology
Xiaoying Li
Huazhong University of Science and Technology
Haining Zhuang
Shanghai Urban Construction Vocational College
Ze Li
Huazhong University of Science and Technology
Min Sun
Shanghai Institute of Technology
Chuang Yu
Shanghai Institute of Technology
Jian Xiong
The Hubei Provincial Key Laboratory of Yeast Function
Ku Li
The Hubei Provincial Key Laboratory of Yeast Function
Jing Hu
The Hubei Provincial Key Laboratory of Yeast Function
Lei Pei
Huazhong University of Science and Technology
Tao Feng
fengtao@sit.edu.cn

Shanghai Institute of Technology

Article

Keywords: kokumi peptide, calcium-sensing receptor, molecular dynamics simulation, taste-related behavior, electroencephalography

Posted Date: November 20th, 2026

DOI: https://doi.org/10.21203/rs.3.rs-11178374/v1

License: This work is licensed under a Creative Commons Attribution 4.0 International License.
Read Full License

Additional Declarations: No competing interests reported.

A Novel Kokumi Peptide RSQPVGV from Yeast Extract via CaSR-Mediated Taste Enhancement

Haofeng Lao‡[a,c], Xiaoying Li‡[b], Haining Zhuang[e], Ze Li[b], Min Sun [a], Chuang Yu [a], Jian Xiong[d], Ku Li[d], Jing Hu[d], Tao Feng*[a], Lei Pei*[b]

[a]School of Perfume and Aroma Technology, Shanghai Institute of Technology, 100 Haiquan Road, Shanghai, 201418, China

[b]Department of Neurobiology, School of Basic Medicine, Tongji Medical College, Huazhong University of Science and Technology, Wuhan, 430030, China.

[c]Institute of Engineering Food, College of Life Sciences, Shanghai Normal University, Shanghai, 201418, China.

[d]The Hubei Provincial Key Laboratory of Yeast Function, 443003, China.

[e]School of Food and Tourism, Shanghai Urban Construction Vocational College, Shanghai, 201415, China.

‡ Haofeng Lao and Xiaoying Li contributed equally to this work as co-first authors.

*Corresponding Authors

Professor Lei Pei, Department of Neurobiology, School of Basic Medicine, Tongji Medical College, Huazhong University of Science and Technology, Wuhan, 430030, People's Republic of China. E-mail: peilei@hust.edu.cn

Professor Tao Feng, School of Perfume and Aroma Technology, Shanghai Institute of Technology, No. 100, Haiquan Road, Shanghai 201418, People's Republic of China. E-mail: fengtao@sit.edu.cn

Abstract

Kokumi peptides enhance food palatability, often via the calcium-sensing receptor (CaSR). We identified candidate peptides from yeast extract using LC–MS/MS and high-throughput molecular docking to CaSR. Molecular dynamics confirmed the novel peptide RSQPVGV formed a stable CaSR complex, and surface plasmon resonance confirmed direct binding (KD = 1.91×10^{-5} M). Human sensory evaluation showed RSQPVGV (1 g/L) significantly enhanced kokumi, salty, and umami intensities of a monosodium glutamate–NaCl solution (MNS). Electronic tongue analysis confirmed increased richness. Mouse behavioral assays revealed RSQPVGV enhanced MNS responses and increased umami-evoked neural activation in the gustatory cortex. Human EEG recordings showed RSQPVGV alone had minimal cortical responses but significantly increased MSG-evoked P300 amplitudes and β-band power, indicating enhanced umami processing. These findings identify RSQPVGV as a novel yeast-derived kokumi peptide, providing multiscale evidence for its taste-enhancing activity, CaSR-binding, and taste-related neural modulation.

Keywords: kokumi peptide; calcium-sensing receptor; molecular dynamics simulation; taste-related behavior; electroencephalography

1. Introduction

Taste perception is a major determinant of food palatability. Beyond the five basic tastes—sweet, sour, salty, bitter, and umami—the sensory attribute kokumi has received increasing attention since kokumi-active compounds were first characterized in garlic extracts (Ueda et al., 1990). Although these compounds have little intrinsic taste, they enhance flavor intensity, continuity, thickness, and mouthfulness when incorporated into food matrices (Li et al., 2024; Ueda et al., 1997). They can also enhance salty and umami sensations, suggesting potential applications in sodium-reduced foods. Many naturally occurring kokumi compounds are food-derived peptides or amino acid derivatives (Xu et al., 2018).

Kokumi perception is thought to involve activation of the calcium-sensing receptor (CaSR) expressed in taste bud cells (Maruyama et al., 2012). Human and murine CaSR exhibit similar responses to kokumi peptides, suggesting conservation of CaSR-dependent signaling between species (Guo et al., 2021). Mouse models can therefore complement human sensory studies by enabling behavioral and neurobiological investigation of kokumi perception (Yamamoto et al., 2025).

Yeast extract, produced from edible yeast by autolysis or enzymatic hydrolysis, is rich in flavor-active compounds and exhibits pronounced kokumi-enhancing properties. Oligopeptides with molecular masses below 1,000 Da have been identified as major contributors to its kokumi activity (Hollebrands et al., 2026). Ten yeast-derived peptides were subsequently shown to enhance umami, saltiness, and thickness in model chicken soup, and molecular simulations predicted stable interactions between these peptides and CaSR (Liu et al., 2015; Chang et al., 2022). Additional kokumi peptides isolated from yeast extract include glutathione, EDFFVR, and IQGFK (Wang et al., 2022; Lao

et al., 2024). Nevertheless, the structure–activity relationships of yeast-derived kokumi peptides and their interactions with CaSR remain insufficiently characterized.

Molecular docking and molecular dynamics simulations have increasingly been used to screen kokumi peptides and investigate their receptor interactions (Yi et al., 2025). However, conventional docking studies generally examine small candidate sets because their workflows involve multiple software packages and labor-intensive procedures (Li et al., 2022). Prescreening based on databases, previously reported sequences, or amino acid composition may improve efficiency but can exclude potentially active peptides (An et al., 2023). Moreover, computational predictions of peptide–CaSR interactions often lack experimental validation.

To address these limitations, we developed a locally implemented, Python-based high-throughput docking pipeline to screen peptides identified in yeast extract for potential CaSR binding. Selected peptide–CaSR interactions were characterized by molecular dynamics simulations and surface plasmon resonance. Taste-enhancing activity and associated neural responses were subsequently evaluated using human sensory assessment, electronic tongue analysis, human electroencephalography, and behavioral and neurobiological assays in mice. This integrated approach aimed to identify novel kokumi peptides and clarify the molecular and sensory basis of their taste-enhancing effects.

2. Materials and Methods

2.1. Chemicals

Yeast extract is provided by Angel Yeast Co., Ltd. Food-grade sodium chloride, monosodium glutamate, sucrose, citric acid, and caffeine are purchased from H-BIO

Biotechnology Co., Ltd. (Guangdong, China). Glutathione (GSH, purity ≥98%) is obtained from Sigma-Aldrich (Germany).

2.2. Peptide Sequence Identification by LC-MS/MS

The yeast extract is dissolved in water and centrifuged, and the supernatant is collected for desalting using ZipTip C18 tips, followed by vacuum drying. The desalted samples are reconstituted in an acetonitrile–water solution containing formic acid and analyzed using a Thermo EASY-nLC system coupled to a Q Exactive Plus mass spectrometer. Peptide separation is performed on a 75μm × 150mm Acclaim PepMap RSLC C18 column (2μm, 100 Å) with mobile phases consisting of 0.1% formic acid in water (A) and 0.1% formic acid in 80% acetonitrile (B), using a 60 min linear gradient.

Full MS scans are acquired at a resolution of 120,000 over an m/z range of 350–1550. Data-dependent MS/MS acquisition is performed in Top20 mode with a resolution of 50,000 and a normalized collision energy (NCE) of 32. Raw data are processed using PEAKS software and searched against the UniProt database with no enzyme specificity. The precursor and fragment mass tolerances are set to 20 ppm and 0.05 Da, respectively. Dynamic modifications include methionine oxidation and N-terminal acetylation, and peptide identification is performed by combining database searching with de novo sequencing.

2.3. In Silico Molecular Simulations

An automated molecular-simulation pipeline (batch_docking.py) was developed locally in Python 3.9 to integrate peptide modeling, energy minimization, file conversion, molecular docking, interaction analysis, and statistical processing. A total of 4,772 peptides were analyzed. Peptide structures were generated using

ChemBioDraw3D and energy-minimized with the MM2 molecular mechanics method. The optimized structures were saved in PDB format and converted to PDBQT format using Open Babel 3.1.1.

Human CaSR was selected as the docking receptor based on previous studies and obtained from the RCSB Protein Data Bank (PDB ID: 5K5S) (Lao et al., 2024). Because the structure contains symmetric A and B chains, chain B was removed in PyMOL and chain A was retained for docking. Native ligands and water molecules were deleted, and polar hydrogens were added. Molecular docking was performed using AutoDock Vina 1.2.3. The docking grid encompassed the CaSR Venus flytrap (VFT) domain, corresponding to Pro22–Ile528 (Hendy et al., 2013). Three binding poses were generated for each peptide, and the pose with the lowest predicted binding energy was selected for subsequent analysis.

The selected peptide–CaSR complexes were visualized and prepared in PyMOL, and their molecular interactions were analyzed using the Protein–Ligand Interaction Profiler (PLIP) (Adasme et al., 2021). Hydrophobic interactions, hydrogen bonds, salt bridges, π–π stacking, π–cation interactions, and halogen bonds were identified. For each peptide, the interacting residues, interaction types, and predicted binding energies were recorded, statistically analyzed, and exported to Microsoft Excel for further processing.

Molecular dynamics (MD) simulations were performed according to the method of Cao et al. using GROMACS 2022 (Cao et al., 2023). The docking-selected complexes of RSQPVGV and GSH were used as the initial structures. Protein topologies were generated with pdb2gmx, and ligand topologies were obtained from the SwissParam server. Protein and ligand parameters were combined using the CHARMM36-jul2021 force field. Each complex was placed at the center of a cubic

simulation box with a minimum distance of 1.5 nm between the complex and the box edges. The box was solvated with the TIP3P water model, and sodium and chloride ions were added to achieve an ionic strength of 0.15 M.

The systems were energy-minimized for 50,000 steps using the steepest-descent algorithm. Equilibration was then performed for 2 ns under constant-volume and constant-temperature (NVT) conditions at 300 K, followed by 1 ns under constant-pressure and constant-temperature (NPT) conditions at 1 bar. Production MD simulations were subsequently conducted for 100 ns with a 2-fs integration time step. The stability and structural properties of the complexes were evaluated by calculating the root-mean-square deviations (RMSDs) of the protein–ligand complexes and protein backbones, the total number of hydrogen bonds, and solvent-accessible surface areas (SASAs). Free-energy landscape maps were generated using the GROMACS tools g_sham and xpm2txt.py.

2.4. Solid-Phase Synthesis of RSQPVGV

The peptide RSQPVGV is synthesized by Nanjing TGpeptide Biotechnology Co., Ltd. using a solid-phase peptide synthesis strategy with acetate as the solvent. The peptide is assembled stepwise from the N-terminus to the C-terminus. The molecular weight and purity of the synthesized peptide are verified by high-performance liquid chromatography (HPLC) and liquid chromatography–mass spectrometry (LC–MS), confirming consistency with the theoretical molecular weight and a purity of ≥ 98%.

2.5. Surface Plasmon Resonance Analysis

Surface plasmon resonance (SPR) experiments were performed using a CM5 sensor chip and a Biacore system. Recombinant human CaSR extracellular domain

(residues 20–601; UniProt ID: P41180) was purchased from CUSABIO. The protein was expressed in Escherichia coli with an N-terminal GST tag, purified by affinity chromatography, supplied in phosphate-buffered saline (PBS; pH 7.4), and stored at −20◦C. Protein purity and molecular weight were verified by SDS–PAGE before use.

The CM5 chip surface was activated by injecting an EDC/NHS mixture at 10μL/min for 420 s. CaSR, diluted to 20 μg/mL in 10 mM sodium acetate buffer (pH 4.5), was immobilized on the sample flow cell to a level of approximately 13,400 response units (RU). The reference flow cell was left unmodified for background correction. Unreacted carboxyl groups were blocked with ethanolamine. In separate experiments, GSH and RSQPVGV were immobilized on CM5 chips under the same activation and blocking conditions, yielding immobilization levels of approximately 12,600 RU.

For peptide–CaSR binding measurements, GSH and RSQPVGV were prepared at concentrations of 1.56–100 μM in PBS containing the required concentrations of DMSO and Tween-20. The peptide solutions were injected over both CaSR-immobilized and reference flow cells in order of increasing concentration at a flow rate of 20μL/min. Association and dissociation phases were monitored for 100 and 180 s, respectively. The sensor surface was regenerated with glycine–HCl after each injection.

To evaluate the effect of the CaSR antagonist NPS-2143, CaSR was preincubated with NPS-2143 at 0, 12.5, 25, 50, 100, or 200 μM for 30 min at room temperature. The resulting mixtures were injected over sensor surfaces immobilized with GSH or RSQPVGV using the same flow rate, association and dissociation times, and regeneration procedure described above.

Binding responses were recorded in real time as RU. Signals from the reference flow cell were subtracted automatically, and the resulting sensorgrams were exported

for further processing in GraphPad Prism. Sensorgrams were subjected to background correction and baseline normalization, and equilibrium dissociation constants (KD) were calculated by fitting the concentration-dependent binding curves. The processed data were used for statistical analysis and graphical presentation.

2.6. Sensory Evaluation

Sensory evaluations were approved by the Ethics Committee of Shanghai Institute of Technology and conducted with minor modifications based on previously reported methods (Zhao et al., 2022). Eight trained panelists (four men and four women; 22–28 years old) were recruited in accordance with ISO 8586:2014. All panelists reported normal taste and olfactory function and had received at least one year of professional sensory training. Before the experiments, they completed weekly triangle-test training for 3 consecutive months using solutions representing sourness (0.025% citric acid), sweetness (0.1% sucrose), bitterness (0.0025% quinine), saltiness (0.25% NaCl), umami (0.06% MSG), and kokumi (clear chicken broth containing 0.1% GSH). All participants provided informed consent.

Evaluations were conducted in individual booths at 23±2◦C under uniform warm-yellow lighting. Samples were equilibrated to 30◦C in a water bath and served in disposable 30-mL cups containing 10 mL of sample. Each sample was assigned a randomly generated three-digit code and presented in a randomized, balanced order. Panelists sipped each sample, rotated it in the mouth for 10 s, and expectorated it. Nose clips were worn throughout the evaluation to minimize olfactory effects. Between samples, panelists rinsed their mouths twice with purified water and rested for approximately 5 min.

Taste thresholds were determined according to GB/T 12311-2012, with modifications based on published procedures (Glabasnia et al., 2006). A taste-dilution method combined with a three-alternative forced-choice (3-AFC) test was used. GSH and RSQPVGV were dissolved in deionized water containing 1% MSG and 0.3% NaCl and serially diluted twofold from an initial concentration of 1 g/L. At each dilution, panelists identified the peptide-containing sample among three coded samples, comprising one peptide-containing sample and two corresponding carrier controls. After the last concentration correctly identified by each panelist, testing continued at lower concentrations. When a panelist gave incorrect responses at two consecutive dilution levels, the concentration of the preceding dilution was recorded as that panelist's threshold. The mean threshold across all panelists was used as the group threshold. Descriptive sensory evaluation was subsequently performed at the corresponding peptide concentrations.

For flavor-profile analysis, GSH and RSQPVGV were added separately to MNS at 1g/L. Panelists evaluated the carrier solution and peptide-containing samples using a five-point intensity scale ranging from 0 (not perceived) to 5 (very strong). Sourness, sweetness, bitterness, saltiness, umami, and kokumi were evaluated for each sample. Each panelist assessed every sample in triplicate. The mean of the three evaluations was calculated for each panelist, and the final intensity score for each attribute was calculated as the mean across all panelists.

2.7. Electronic Tongue Analysis

Electronic tongue analysis is performed using a taste sensing system (TS-5000Z, INSENT Inc., Japan) equipped with lipid membrane sensors for umami, sourness, sweetness, saltiness, bitterness, and astringency, together with aftertaste indicators

including Aftertaste-B, Aftertaste-A, and Richness. Sensors are conditioned and calibrated following the manufacturer's instructions, and all measurements are performed at 25 °C. GSH and RSQPVGV are added to the MNS carrier solution at 1 g/L and analyzed alongside the blank carrier solution. During measurement, sensor responses are first recorded in a standard reference solution, followed by recording in the sample solution to obtain the initial taste signal. After rinsing with the reference solution, the residual sensor response is measured and defined as the aftertaste signal. After each measurement, sensors are thoroughly cleaned using the corresponding membrane-specific washing solutions.

2.8. Mice Behavioral Experiments

Female wild-type C57BL/6J mice from the same production batch were purchased from Shulabao Biotechnology Co., Ltd. All animal procedures complied with the Regulations for the Administration of Laboratory Animals of the People's Republic of China and the Guidelines for the Care and Use of Laboratory Animals of Huazhong University of Science and Technology. The study was approved by the Animal Ethics Committee of Huazhong University of Science and Technology. Mice were housed at 22±1◦C and approximately 50% relative humidity under a 12-h light/12-h dark cycle, with no more than five mice per cage. Bedding was changed once or twice weekly, and standard chow and water were provided ad libitum.

Two-bottle preference (TBP) tests were conducted according to protocols recommended by the Monell Chemical Senses Center (Chen et al., 2017). Identical 60-mL plastic bottles fitted with stainless-steel sipper tubes containing ball bearings were used to provide consistent tactile stimulation during licking. The bottles were positioned at the center of each cage, with the sipper tips approximately 3 cm apart. Mice were

habituated to the two-bottle apparatus for 2 weeks. Subsequently, ten healthy 8-week-old female mice with comparable body weights were housed individually and acclimated to the apparatus for an additional 3 days. Food remained available throughout acclimation, and water was withheld for 24 h before testing. Behavioral experiments began at 8:00 a.m. the following day.

For the 24-h TBP tests, experimental assignments are provided in Supplementary Table 1. Equal initial quantities of solutions A and B were added to the two bottles, which were weighed before placement in the cages. Bottle positions were randomized among mice and exchanged after 12 h to minimize side bias. After 24 h, the bottles were reweighed, and solution consumption was calculated from the weight difference. The preference for solution B was calculated for each mouse as

$$P_i = \frac{\Delta B_i}{\Delta A_i + \Delta B_i}$$

where P_i is the preference score for mouse i, and ΔA_i and ΔB_i are the amounts of solutions A and B consumed, respectively. The mean preference score across the ten mice was used for statistical analysis:

$$P_{avg} = \frac{1}{10}\sum_{i=1}^{10} Pi$$

The seven mice exhibiting the strongest preference for peptide-enhanced taste stimuli in the 24-h TBP experiments were selected for the 30-min TBP tests. Experimental assignments are provided in Supplementary Table 2. Equal initial volumes of the two solutions were used, and bottle positions were randomized and exchanged after 15 min. For Group 1, solution consumption was determined from the difference between the initial and final bottle weights. For Groups 2 and 3, licking behavior was recorded using an Arduino-controlled digital signal-acquisition system connected to both bottles, together with continuous video recording [54]. The number

of licks directed toward each solution was quantified for every mouse during the 30-min test and used for subsequent analysis.

2.9. Fiber Photometry Recording of Calcium Signals in the Mouse Gustatory Cortex

Mice were anesthetized by intraperitoneal injection of a mixture containing 2% chloral hydrate and 10% urethane at 0.01mL/g body weight. After loss of the righting reflex, the animals were placed in a stereotaxic apparatus and secured with ear bars, an incisor bar, and a nose clamp. Erythromycin ophthalmic ointment was applied to both eyes, and the scalp was disinfected with 75% ethanol before incision. The periosteum was removed to expose the bregma and lambda landmarks. Skull leveling was performed by measuring the dorsoventral coordinates at multiple points around bregma and adjusting the skull until the anterior–posterior and medial–lateral deviations were no greater than 0.03 mm.

A glass micropipette connected to a microsyringe was mounted on the stereotaxic injector. After removal of air bubbles, 300nL of GCaMP6s virus was aspirated at 60 nL/min, and the injection needle was positioned above the target site in the insular cortex (AP, +1.90 mm; ML, ±2.70 mm; DV, +3.00 mm). A small burr hole was drilled in the skull, and 200 nL of viral suspension was injected at 25nL/min. The needle was left in place for 10 min after injection and then withdrawn slowly to minimize backflow. An optical fiber was implanted at the recording site according to the experimental configuration.

Fiber photometry recordings were performed 3 weeks after viral injection to allow sufficient GCaMP6s expression. Before recording, mice were habituated to the experimental environment and natural-posture drinking procedure for at least 2 weeks. During testing, the implanted optical fiber was connected to the fiber-photometry

system through a patch cable. Calcium-dependent fluorescence was excited with a 470-nm laser, whereas a 410-nm isosbestic laser was used to correct for motion-related fluorescence changes. The modulation frequency was 15 Hz, the exposure time was 30 ms, and the optical power at the fiber tip was maintained at 20–30μW. Fluorescence signals were recorded while mice consumed the designated solutions. Raw signals were processed and normalized using InperDataProcess software to align baseline fluorescence across animals and reduce inter-animal variability before statistical analysis.

After completion of the recordings, viral expression and recording-site placement were histologically verified. Mice were deeply anesthetized using the procedure described above and perfused transcardially with 100 mL of PBS at approximately 80 rpm, followed by 50 mL of 4% paraformaldehyde (PFA). Successful perfusion was confirmed by hepatic blanching and the absence of pulmonary edema. Brains were removed, post-fixed in 4% PFA for 24 h, and cryoprotected sequentially in 10%, 20%, and 30% sucrose solutions. Coronal sections were prepared using a Leica cryostat at −20◦C, with 15-μm-thick sections collected into antifreeze solution. Sections were examined by fluorescence microscopy to verify GCaMP6s expression and the viral injection sites.

2.10. Human EEG-Based Gustatory Experiment

Eight healthy volunteers (four men and four women; mean age, 24.5±2.1 years) participated in the study. All participants were right-handed, nonsmokers, and free from olfactory or gustatory disorders, neurological disease, and long-term medication use. They abstained from alcohol, spicy foods, and caffeinated beverages for at least 24 h before testing. The study protocol was approved by the Ethics Committee of Huazhong

University of Science and Technology, and written informed consent was obtained from all participants. All procedures conformed to the Declaration of Helsinki.

Four test solutions were prepared using food-grade reagents and distilled water: distilled water, 0.1% RSQPVGV, 0.6% MSG, and a mixture containing 0.1% RSQPVGV and 0.6% MSG. Solutions were prepared immediately before testing and maintained at 30◦C in a thermostatic water bath.

Experiments were conducted in a sound-attenuated, electromagnetically shielded laboratory. Participants were seated in a comfortable semireclined position and instructed to remain relaxed throughout the experiment. EEG signals were recorded using a 19-channel Ag/AgCl electrode cap positioned according to the international 10–20 system (Fp1, Fp2, F7, F3, Fz, F4, F8, T3, C3, Cz, C4, T4, T5, P3, Pz, P4, T6, O1, and O2). The bilateral mastoids (A1 and A2) served as reference electrodes, and AFz was used as the ground. Electrode impedance was maintained below 5kΩ. Each solution was presented in randomized order, and each participant completed 10 trials per solution. In each trial, participants first rested with their eyes closed for 30 s to establish a baseline. Subsequently, 10 mL of the test solution was delivered into the mouth while EEG recording continued. Participants gently swished the solution for 10 s with minimal facial movement and then expectorated it. The mouth was rinsed three times with distilled water, followed by a 5-min interval before the next trial.

EEG data were acquired using a Nihon Kohden EEG-1200C amplifier at a sampling rate of 1,000 Hz. Data were preprocessed in MATLAB using EEGLAB v2021. Signals were band-pass filtered from 0.5 to 50 Hz and subjected to an additional 50-Hz notch filter to remove power-line interference. Ocular and muscular artifacts were removed by independent component analysis. Continuous recordings were segmented into epochs from −200 to 800 ms relative to stimulus onset and baseline-corrected using

the −200 to 0 ms prestimulus interval. Epochs with voltage amplitudes exceeding ± 100μV were rejected automatically.

Statistical analyses were performed using GraphPad Prism 9.0. Data normality was assessed using the Shapiro–Wilk test. Differences among treatments were evaluated by one-way repeated-measures analysis of variance, with solution type as the within-subject factor. Greenhouse–Geisser correction was applied when the sphericity assumption was violated, and Bonferroni-adjusted post hoc comparisons were conducted when appropriate. Statistical significance was defined as $p<0.05$.

2.11. Statistical analysis

All experiments are performed in triplicate, and data are presented as mean values. Statistical analysis is conducted using SPSS 19.0 (SPSS Inc., Chicago, IL, USA). Differences among groups are evaluated by one-way analysis of variance (ANOVA) followed by Duncan's multiple range test. Statistical significance is defined at $*p < 0.05$ and $**p < 0.01$, $***p < 0.001$ and $****p < 0.0001$.

3. Results and discussion

3.1. LC–MS/MS peptide identification and construction of the virtual screening library

To systematically identify potential kokumi peptides from yeast extract, a comprehensive peptide library was first established by LC–MS/MS. Because peptide structure and chain length can influence kokumi activity and receptor binding, the identified sequences were filtered before molecular docking against CaSR. As shown in Fig. 1a, the yeast extract was desalted and purified before LC–MS/MS analysis, and the resulting total ion chromatogram is presented in Fig. 1b. De novo sequencing

identified 8,474 peptides, including 2,557 acetylated or oxidized peptides and 5,917 unmodified linear peptides. Because linear peptides represent the largest reported class of kokumi-active peptides (approximately 45.1%) (He et al., 2024), unmodified linear peptides were selected for further screening. The longest kokumi peptide reported to date comprises 14 amino acid residues (RGENESEEEGAIVT) (Zhang et al., 2019). Accordingly, 4,772 peptides comprising 5–14 residues were retained and subjected to high-throughput molecular docking (Fig. 1c). Among these, 2,608 were successfully docked to CaSR and retained for binding-site analysis and further screening. These results established a focused library of yeast-derived peptides for the subsequent identification of potential CaSR-binding kokumi candidates.

3.2. High-throughput docking identifies RSQPVGV as a candidate CaSR-binding peptide

To prioritize potential kokumi peptides, the 4,772-peptide library was screened against the Venus flytrap (VFT) domain of CaSR. The effects of peptide length and receptor-interacting residues were analyzed to characterize peptide–CaSR binding patterns and identify candidates for further validation. Each peptide was docked three times, and the pose with the lowest predicted binding energy was retained. The absolute value of this energy was defined as the docking score, with higher scores indicating stronger predicted binding (Lao et al., 2024). Peptides with scores below 5 were considered not to meet the docking criterion and were excluded (Rentzsch et al., 2015). Overall, 2,608 peptides had docking scores of at least 5. The number of screened peptides varied by chain length and was highest for octapeptides (Fig. 2a). Docking success generally decreased with increasing peptide length, particularly beyond eight residues. Peptides

containing 5–8 residues exhibited success rates above 80%, whereas longer peptides showed a progressive decline.

Analysis of the 2,608 successfully docked complexes identified hydrogen bonds, hydrophobic interactions, salt bridges, π–π stacking, and π–cation interactions as the principal intermolecular forces. Residues involved in at least 1,000 interactions are presented in Fig. 2b, while less frequently involved residues are listed in Supplementary Table 3. The ten most frequently interacting CaSR residues were Arg66, Asn102, Tyr218, Ser272, Ala298, Val104, Asp216, Asp217, Phe42, and Thr145. Mapping residues according to interaction frequency (1,000–2,000, 2,000–3,000, 3,000–4,000, and ⩾4,000 interactions) showed that the docking poses were concentrated within a common cavity of the CaSR VFT domain (Fig. 2c). The most frequently interacting residues were located near the center of this cavity and collectively surrounded the docked peptides, whereas less frequently involved residues were distributed more peripherally.

Heptapeptides exhibited the highest docking success rate (93.4%) and were therefore prioritized for further screening. Among the 654 successfully docked heptapeptides, 55 had scores of 5–6, 161 scored 6–7, 276 scored 7–8, 143 scored 8–9, and 19 scored 9–10 (Fig. 2d). RSQPVGV achieved the highest docking score among these candidates, indicating the strongest predicted interaction with CaSR. Its sequence assignment was supported by the corresponding MS/MS spectrum (Fig. 2e), and it was therefore selected for subsequent computational and experimental evaluation.

Collectively, these results reveal a peptide-length-dependent pattern of predicted CaSR binding, identify a recurrent interaction cavity within the VFT domain, and support RSQPVGV as a promising CaSR-binding kokumi peptide candidate.

3.3. RSQPVGV exhibits stable predicted binding to the CaSR VFT domain

To characterize the interaction of RSQPVGV with CaSR and assess the stability of the predicted complex, molecular docking and 100-ns molecular dynamics (MD) simulations were performed. Glutathione (GSH), a recognized kokumi peptide, was included as a positive control to provide a reference for comparison. RSQPVGV and GSH yielded docking scores of 9.929 and 6.031, corresponding to predicted binding energies of −9.929 and −6.031 kcal/mol, respectively. Both peptides occupied the same cavity within the CaSR Venus flytrap (VFT) domain (Fig. 3a,b). GSH formed hydrogen bonds with Arg66, Asn102, Ser147, Ala168, Gly273, and Ala298, together with a salt bridge involving Arg66 (Fig. 3a). By comparison, RSQPVGV formed a more extensive interaction network (Fig. 3b), including two hydrogen bonds with each of Arg66, Asn102, and Asp216 and single hydrogen bonds with Thr103, Val104, Thr145, Gly146, Ser147, Gly148, Gln245, Ser272, and Gly273. Hydrophobic interactions were additionally observed with Phe42, Trp70, Thr145, Tyr218, and Ala298.

The dynamic stability of the two complexes was subsequently evaluated by MD simulation. Both systems initially exhibited increased complex and CaSR-backbone root-mean-square deviations (RMSDs), reflecting conformational relaxation from their starting structures (Fig. 3c,d). The RMSD profiles became relatively stable after approximately 20 ns. Between 20 and 60 ns, RSQPVGV–CaSR generally exhibited lower RMSD values than GSH–CaSR. After 60 ns, the complex RMSDs converged at approximately 0.4 nm, while the backbone RMSDs stabilized at approximately 0.3 nm. These profiles indicate that both complexes reached relatively stable conformations during the latter part of the simulations.

The number of peptide–receptor hydrogen bonds decreased during the initial equilibration period and subsequently stabilized (Fig. 3e). From approximately 40 ns

onward, GSH–CaSR maintained approximately three hydrogen bonds, whereas RSQPVGV–CaSR maintained approximately seven, indicating a more extensive and persistent hydrogen-bonding network for RSQPVGV. The solvent-accessible surface areas of both systems decreased initially and stabilized at approximately 265 nm^2 after 40 ns (Fig. 3f), suggesting that both complexes adopted comparably compact conformations.

Free-energy landscapes were constructed using RMSD and radius of gyration as reaction coordinates. GSH–CaSR exhibited a broad, heterogeneous low-energy distribution containing several basins (Fig. 3g), indicating greater conformational variability. In contrast, RSQPVGV–CaSR displayed a concentrated low-energy region dominated by a single deep basin (Fig. 3h), consistent with a more restricted and stable conformational ensemble. The principal energy minima of both systems nevertheless occurred in similar regions, supporting their predicted occupation of a common CaSR-binding cavity.

Together, these results suggest that RSQPVGV binds within the CaSR VFT-domain cavity through a more extensive interaction network and forms a more conformationally stable predicted complex than GSH, supporting its subsequent experimental validation.

3.4. RSQPVGV directly binds with CaSR

To experimentally validate the predicted interaction between RSQPVGV and CaSR, surface plasmon resonance (SPR) assays were performed using GSH as a positive control. Direct-binding measurements were followed by antagonist assays with NPS-2143 to determine whether peptide–CaSR binding was sensitive to pharmacological inhibition of CaSR (Fig. 4a,b). The molecular masses of synthesized RSQPVGV and

recombinant CaSR agreed with their theoretical values, and their purities were ⩾98% and ⩾90%, respectively (Supplementary Fig. 1).

For direct-binding analysis, CaSR was immobilized on the sensor chip, and GSH or RSQPVGV was injected at concentrations of 1.56–100 μM. Both peptides produced concentration-dependent SPR responses (Fig. 4c,e). At 100 μM, the response reached approximately 31 response units (RU) for GSH and 62 RU for RSQPVGV. Steady-state fitting yielded equilibrium dissociation constants (K_D) of 1.05×10^{-4} M for GSH and 1.91×10^{-5} M for RSQPVGV (Fig. 4d,f). The approximately 5.5-fold lower K_D of RSQPVGV indicates a higher apparent affinity for CaSR than GSH, consistent with the molecular docking predictions.

The sensitivity of these interactions to NPS-2143 was subsequently examined using immobilized GSH or RSQPVGV and CaSR preincubated with increasing antagonist concentrations. NPS-2143 progressively reduced the SPR responses of CaSR to both peptides in a concentration-dependent manner (Fig. 4g,h). At 100 μM NPS-2143, the binding signals approached baseline, with little additional reduction at 200 μM, indicating near-complete inhibition under the tested conditions.

Cumulatively, these results demonstrate that RSQPVGV binds directly to CaSR with a higher apparent affinity than GSH and that this interaction is sensitive to the CaSR antagonist NPS-2143.

3.5. Sensory and electronic-tongue validation of the taste-enhancing effects of RSQPVGV

To determine whether the confirmed interaction between RSQPVGV and CaSR translated into perceptible taste enhancement, sensory evaluation and electronic-tongue analysis were performed using GSH as a positive control. MNS was used as the

evaluation medium because its basic taste components enable the kokumi-enhancing effects of peptides to be assessed without requiring the peptides themselves to possess a strong basic taste (Chun et al., 2014). The overall experimental workflow is illustrated in Fig. 5a.

The taste thresholds of GSH and RSQPVGV in MNS were 0.31 mmol/L (9.57×10^{-2} g/L) and 0.37 mmol/L (2.72×10^{-1} g/L), respectively (Table 1). The threshold measured for GSH was comparable to its previously reported value in monosodium glutamate solution (0.33 mmol/L) (Ueda et al., 1997). At 1 g/L (0.1%, w/v), both peptides altered the sensory profile of MNS primarily by enhancing saltiness, umami, and kokumi, while exerting little influence on sourness, sweetness, or bitterness (Fig. 5b). Quantitative evaluation of the three enhanced attributes confirmed that both peptide-containing samples received higher scores than MNS alone (Fig. 5c). RSQPVGV produced the greatest kokumi intensity among the tested samples, indicating a pronounced taste-enhancing effect.

Electronic-tongue analysis was subsequently conducted to provide an instrumental assessment of these sensory changes (Fig. 5d). Because kokumi peptides enhance taste perception through physiological mechanisms rather than directly increasing the concentrations of salt or umami compounds, the Richness parameter was used as the principal indicator of kokumi-related effects (Tahara et al., 2013; Brown et al., 1993; Nishimura et al., 2019; Kobayashi et al., 2010). Compared with MNS alone, supplementation with GSH or RSQPVGV significantly increased the Richness value (Fig. 5e; $P<0.01$ and $P<0.001$, respectively). RSQPVGV yielded the highest Richness value, consistent with its stronger kokumi-enhancing effect in the sensory evaluation.

These results indicate that RSQPVGV enhances the saltiness, umami, and particularly kokumi characteristics of MNS, with sensory and electronic-tongue measurements consistently supporting its potential as a kokumi-active peptide.

3.6. Kokumi peptides enhance taste preference in mice through a CaSR-sensitive mechanism

To determine whether the taste-enhancing effects observed in sensory evaluation translated into altered ingestive behavior, two-bottle preference tests were performed in mice (Fig. 6a). MNS concentration–preference relationships were first established to select a subthreshold test medium, after which the effects of GSH and RSQPVGV on MNS and individual basic tastes were evaluated. The CaSR antagonist NPS-2143 was subsequently used to investigate the potential involvement of CaSR in peptide-induced taste enhancement.

In the 24-h preference test, mice showed no significant preference for 0.2–0.6× MNS over water (Fig. 6b). Preference became significant at 0.8× MNS and remained elevated at 1.0× and 1.2×, with a preference score of 0.61±0.08 at 0.8× ($P<0.001$). At higher concentrations, preference declined; no significant preference was observed at 1.4×, while the scores decreased to 0.48±0.05 and 0.43±0.08 at 1.6× and 1.8× MNS, respectively. Therefore, 0.6× MNS, which was immediately below the concentration eliciting significant preference, was selected to assess peptide-mediated enhancement.

Neither 0.1% GSH nor 0.1% RSQPVGV in water elicited a significant preference over water, indicating that the peptides alone were insufficient to induce preferential consumption (Fig. 6c,d). In contrast, adding GSH or RSQPVGV to 0.6×MNS increased preference relative to 0.6× MNS alone. The preference scores were 0.59±0.07 for GSH ($P<0.001$) and 0.55±0.05 for RSQPVGV ($P<0.05$). To identify the basic tastes enhanced

by these peptides, the individual components of 0.6× MNS—0.6% MSG and 0.18% NaCl—were evaluated separately. Both GSH and RSQPVGV enhanced preference for 0.6% MSG, producing preference scores of 0.69±0.13 and 0.66±0.08, respectively ($P<0.0001$; Fig. 6c,d). GSH also significantly enhanced preference for 0.18% NaCl ($P<0.05$), whereas RSQPVGV had no significant effect, even when tested at higher concentrations of 0.2%, 0.5%, and 1% (data not shown). Both peptides additionally increased preference for 0.1 M sucrose ($P<0.05$), suggesting enhancement of sweetness.

The involvement of CaSR was subsequently investigated using a 30-min licking assay because shorter tests can minimize the potential loss of antagonist activity (Yamamoto et al., 2022; Ebenso et al., 2021). NPS-2143 was tested at 0.005%, with 2% ethanol used as the vehicle. Neither the vehicle nor NPS-2143 significantly altered drinking preference relative to water (Supplementary Fig. 2), although NPS-2143 reduced total fluid consumption. The latter observation was considered when interpreting its inhibitory effects.

Because both peptides most strongly enhanced preference for MSG, 0.6% MSG was selected for the antagonist assay. During the 1,800-s test, cumulative licking increased rapidly within the first 300 s and more gradually thereafter (Fig. 6e,f). Adding 0.1% GSH increased the total number of licks from 492.07±294.46 for MSG alone to 1233.86±520.55, while adding 0.1% RSQPVGV increased the count from 516.93±94.05 to 1070.43±336.86. Addition of 0.005% NPS-2143 significantly attenuated these responses. Total licking decreased to 733.00±411.82 for the GSH-containing solution and 679.14±65.45 for the RSQPVGV-containing solution ($P<0.0001$). However, licking remained higher than that elicited by MSG alone, indicating partial rather than complete suppression of the peptide-associated enhancement (Fig. 6g,h).

Taken together, these results suggest that GSH and RSQPVGV enhance behavioral preference for umami and sweet solutions, while their differential effects on saltiness suggest distinct taste-modulating profiles; moreover, the attenuation produced by NPS-2143 supports a CaSR-sensitive contribution to their flavor-enhancing activity.

3.7. RSQPVGV enhances MSG-evoked calcium responses in the mouse gustatory cortex

To determine whether the behavioral taste enhancement produced by RSQPVGV was accompanied by altered central gustatory processing, fiber photometry was used to record calcium activity in the gustatory region of the mouse insular cortex. Responses to distilled water, 0.1% RSQPVGV, 0.6% MSG, and 0.6% MSG plus 0.1% RSQPVGV were compared during licking. Three weeks after viral injection, calcium signals were recorded from water-deprived mice during voluntary consumption of the four solutions (Fig. 7a). Lick-burst onset was synchronized with the fiber-photometry signal, allowing stimulus-evoked fluorescence changes to be aligned and analyzed (Fig. 7b). Histological examination confirmed GCaMP6s expression at the targeted site in the gustatory cortex (Fig. 7c).

The heatmaps and mean fluorescence traces showed that 0.1% RSQPVGV alone induced little change in calcium activity following lick-burst onset (Fig. 7d). The response to 0.6% MSG was also relatively modest (Fig. 7e), whereas the addition of 0.1% RSQPVGV to 0.6% MSG produced a pronounced post-lick increase in fluorescence (Fig. 7f). Overlaying the four response traces further illustrated their differences, and the interval from 0 to 2 s after lick-burst onset was selected for area-under-the-curve (AUC) analysis (Fig. 7g). Quantitative analysis showed no significant difference in AUC between distilled water and 0.1% RSQPVGV alone (Fig. 7h). In

contrast, the AUC for 0.6% MSG plus 0.1% RSQPVGV was significantly greater than that for 0.6% MSG alone ($P<0.05$).

Overall, these results indicate that RSQPVGV alone evokes minimal gustatory cortical activity but significantly enhances the calcium response elicited by MSG, supporting its role as a taste-enhancing rather than an independently taste-active peptide.

3.8. RSQPVGV enhances MSG-evoked cortical gustatory responses in humans

To determine whether RSQPVGV modulates human neural responses to umami stimulation, electroencephalography (EEG) was performed during oral exposure to water, 0.1% RSQPVGV, 0.6% MSG, or 0.1% RSQPVGV plus 0.6% MSG. Event-related potentials (ERPs), time–frequency activity, scalp distributions, and cortical source activity were analyzed to characterize the neural effects of RSQPVGV.

As illustrated in Fig. 8a, each 200-μL sample was delivered after a stable 5-min baseline, retained in the mouth for 10 s, and then expectorated, followed by rinsing and a 5-min baseline-recovery period. Each sample was administered sequentially for 10 trials. Grand-averaged ERPs recorded at the Cz electrode showed N1, N2, and P300 components, with the RSQPVGV–MSG mixture producing the largest overall response (Fig. 8b). Quantitative analyses showed no significant differences between water and RSQPVGV alone for N1, N2, or P300 amplitude (Fig. 8c–e). In contrast, the mixture elicited significantly greater N1, N2, and P300 amplitudes than water ($P<0.05$, $P<0.01$, and $P<0.05$, respectively), whereas MSG alone did not differ significantly from water for these components.

Time–frequency analysis revealed limited spectral modulation following water or RSQPVGV stimulation (Fig. 8f). MSG and the RSQPVGV–MSG mixture induced beta-band event-related synchronization and alpha-band event-related

desynchronization, with the mixture displaying the most pronounced spectral response. Scalp topography showed broadly elevated beta activity following the mixed stimulus (Fig. 8g). Beta power did not differ significantly between water and RSQPVGV alone but was significantly higher following MSG and RSQPVGV–MSG stimulation than following water (both $P<0.0001$; Fig. 8h). Source localization identified activity in gustatory- and reward-related regions, including the insular and orbitofrontal cortices (OFC; Fig. 8i). Quantitative analysis showed that OFC current density did not differ significantly between water and RSQPVGV alone but was significantly higher following MSG ($P<0.05$) and the RSQPVGV–MSG mixture ($P<0.0001$) than following water (Fig. 8j).

Together, these results suggest that RSQPVGV alone evokes little detectable cortical response but enhances the overall neural response to MSG, as reflected by stronger ERP components, spectral modulation, and activation of gustatory and reward-related cortical regions.

3.9. Discussion

This study comprehensively characterizes RSQPVGV, a yeast-derived kokumi-active peptide, through an integrated multidisciplinary approach. Our investigations demonstrate its direct CaSR binding with superior affinity to GSH and significant enhancement of taste perception, particularly with MSG. CaSR antagonist NPS-2143 largely attenuated these effects, confirming a prominent CaSR-dependent mechanism.

Computational screening revealed an inverse relationship between peptide length and CaSR docking success, failing for peptides >14 residues. This aligns with CaSR VFT domain constraints (Li et al., 2022; Wang et al., 2016) and kokumi peptide characteristics (<1,000 Da) (Yang et al., 2025). Arg66 was a crucial interaction hotspot,

with frequent contacts at Asn102, Tyr218, and Ser272 within the central VFT cavity, implicated in kokumi peptide recognition (Xia et al., 2022; Feng et al., 2024; Yamaguchi et al., 2025). While these guide screening, receptor activation requires cooperative multi-point interactions. Length-dependent docking reflects algorithm limitations, serving as a screening metric, not definitive functional proof.

Integrating computational data, RSQPVGV was a top candidate. MD simulations showed RSQPVGV formed a more extensive binding network within the VFT cavity and exhibited superior stability compared to GSH (Feng et al., 2024). SPR validated this, demonstrating RSQPVGV's concentration-dependent CaSR binding with ~5.5-fold higher affinity (KD 1.91×10^{-5} M) than GSH (KD 1.05×10^{-4} M). NPS-2143 inhibited these responses, confirming CaSR involvement. However, SPR measures binding, not functional activation; immobilization artifacts are possible. Further site-directed mutagenesis and cell-based assays are necessary to confirm Arg66's role and delineate RSQPVGV's precise mechanism.

These biophysical interactions translated into pronounced sensory enhancements. Human evaluations showed comparable MNS taste thresholds for GSH and RSQPVGV (0.31 and 0.37 mmol/L). At 1 g/L, both peptides significantly elevated saltiness, umami, and kokumi perception without affecting other basic tastes. RSQPVGV yielded the highest kokumi score and maximized electronic tongue "Richness" (Kobayashi et al., 2010; Li et al., 2023). Given equal mass concentrations differ in molarity, results highlight superior formulation-level performance. The C-terminal VGV motif likely contributes, as GV is a known kokumi enhancer (Perenzoni et al., 2024) and structural analyses highlight its role in CaSR binding (Yamaguchi et al., 2025). Truncated derivative evaluation will clarify its function.

Behavioral assays in mice provided in vivo insights into peptide-mediated taste enhancement. Mice exhibited an inverted U-shaped preference for MNS dilutions, favoring moderate salty–umami blends (Hao et al., 2011; Kuroda, 2022). Both RSQPVGV and GSH significantly increased intake preferences for 0.6× MNS, MSG, and sucrose, confirming kokumi substances amplify existing tastes (Ueda et al., 1997; Yamamoto et al., 2025; Banik et al., 2020). However, GSH enhanced NaCl preference, while RSQPVGV did not, suggesting divergent CaSR ligand taste-modulation, potentially due to structural differences engaging distinct taste-cell signaling axes (Kurihara et al., 2000; Bellisle et al., 1999). Gustatory nerve recordings are needed for verification.

Short-term licking assays confirmed both peptides augmented MSG intake, suppressed by NPS-2143. This 30-minute paradigm supports a peripheral site of action. Incomplete antagonist inhibition, alongside reduced baseline fluid intake, suggests nonspecific motivational effects, incomplete target blockade, or additional pathways (e.g., GPRC6A, purinergic signaling) (Ohsu et al., 2010; Brennan et al., 2014; Park et al., 2025). Thus, CaSR is central but operates within a broader network of oral signaling.

Fiber photometry investigated RSQPVGV's impact on central gustatory processing. RSQPVGV alone induced insular cortical calcium dynamics like water; co-administration with MSG robustly elevated post-lick calcium transients compared to MSG alone. This amplification, consistent with umami-responsive neural ensembles (Chen et al., 2011), suggests RSQPVGV enhances central umami representation without spontaneous cortical firing. Peripheral CaSR activation likely triggers IP3-dependent calcium release, depolarization, and ATP-mediated gustatory afferent transmission, potentially synergizing with the T1R1/T1R3 umami receptor (Pluskal et

al., 2018). This cellular cascade remains a working model due to bulk recording limitations.

Human electroencephalography (EEG) provided complementary systems-level insights into cortical responses. RSQPVGV co-administered with MSG generated the most pronounced event-related potentials (ERPs) (N1, N2, P300 amplitudes significantly higher than water). Spectral analyses revealed enhanced beta-band synchronization, alpha-band desynchronization, and elevated orbitofrontal cortex (OFC) current density, indicating active cortical processing and complex flavor integration (Li et al., 2025; Shan et al., 2024; Cui et al., 2023). While a clear numerical trend was observed, statistical separation between mixture and MSG alone was not definitively established in scalp recordings, contrasting with fiber photometry in mice.

This comprehensive study establishes RSQPVGV as a novel kokumi peptide, elucidating its CaSR-binding and taste-enhancing properties across multiple biological levels. Methodological limitations include simplified computational/SPR models, fixed-mass sensory evaluations, behavioral assay confounding, and inherent resolution constraints in fiber photometry/EEG. Future work must prioritize molecular specificity (CaSR mutagenesis targeting Arg66, cell-based assays, nerve recordings, receptor-knockout models). Comprehensive translational evaluations—including molar-matched sensory panels, stability/digestion profiles, and adequately powered human neuroimaging—are crucial for RSQPVGV's commercial realization.

.

4. Conclusion

In summary, this study establishes RSQPVGV as a potent kokumi-active peptide that binds CaSR with superior apparent affinity compared to GSH, substantially amplifying umami-associated sensory, behavioral, and neural processing. Although

pharmacological data highlight a major CaSR-mediated pathway, contributions from alternative signaling routes remain plausible. These convergent multi-level findings position RSQPVGV as a promising natural flavor-modulating candidate and provide a robust methodological framework for discovering and validating novel kokumi peptides.

CRediT authorship contribution statement

Haofeng Lao, Tao Feng, and Lei Pei contributed to the conceptualization of the study, designed the figures, interpreted the data, and drafted and edited the manuscript. **Haofeng Lao** conducted the in silico molecular simulations. **Xiaoying Li** and **Ze Li** carried out the animal behavioral studies and immunohistological experiments. **Haining Zhuang and Tao Feng** prepared the experimental materials and performed the Mass spectrum assays. **Hao Feng Lao**, **Xiaoying Li and Lei Pei** performed the EEG studies and data analysis. **Min Sun** and **Chuang Yu** performed surface plasmon resonance analysis and assisted with data analysis. **Jian Xiong**, **Ku Li** and **Jing Hu** supervised the project and provided final approval of the version to be published. All authors critically reviewed and approved the final manuscript.

Declaration of competing interest

The authors declare that they have no known competing financial interests or personal relationships that could have appeared to influence the work reported in this paper.

Acknowledgements

This work was supported by the National Natural Science Foundation of China (81870932, 81571078, 81200863), Hubei Provincial Health Commission General Project (WJ2023M001), the Hubei Provincial Natural Science Foundation Joint Foundation Key Project (JCZRLH202500876).

Ethics Approval and Consent to Participate

Animal Experiments: All animal procedures and behavioral/fiber photometry experiments involving mice were performed in strict accordance with the guidelines of the Institutional Animal Care and Use Committee (IACUC) of Huazhong University of Science and Technology (Approval No.2023-0125).

Human Subjects: The human sensory evaluation and EEG experiments were approved by the Ethics Committee of Huazhong University of Science and Technology (Approval No. HUST-2023-018). Written informed consent was obtained from all individual participants prior to the experiments.

Data availability

The data that support the findings of this study are available from the

corresponding author upon reasonable request.

References

Adasme, M. F., Linnemann, K. L., Bolz, S. N., Kaiser, F., Salentin, S., Haupt, V. J., & Schroeder, M. (2021). PLIP 2021: Expanding the scope of the protein–ligand

interaction profiler to DNA and RNA. Nucleic Acids Research, 49, W530–W534. https://doi.org/10.1093/nar/gkab294

An, F., Cao, K., Ji, S., Wang, Y., Pan, G., Ma, Y., Zhao, Y., Wu, J., & Wu, R. (2023). Identification, taste characterization, and molecular docking study of a novel microbiota-derived umami peptide. Food Chemistry, 404, 134583. https://doi.org/10.1016/j.foodchem.2022.134583

Banik, D. D., Benfey, E. D., Martin, L. E., Kay, K. E., Loney, G. C., Nelson, A. R., Ahart, Z. C., Kemp, B. T., Kemp, B. R., Torregrossa, A.-M., et al. (2020). A subset of broadly responsive type III taste cells contribute to the detection of bitter, sweet and umami stimuli. PLoS Genetics, 16, e1008925. https://doi.org/10.1371/journal.pgen.1008925

Bellisle, F. (1999). Glutamate and the umami taste: Sensory, metabolic, nutritional and behavioural considerations. A review of the literature published in the last 10 years. Neuroscience & Biobehavioral Reviews, 23, 423–438. https://doi.org/10.1016/S0149-7634(98)00043-8

Brennan, S. C., Davies, T. S., Schepelmann, M., & Riccardi, D. (2014). Emerging roles of the extracellular calcium-sensing receptor in nutrient sensing: Control of taste modulation and intestinal hormone secretion. British Journal of Nutrition, 111, S16–S22. https://doi.org/10.1017/S0007114513002250

Brown, E. M., Gamba, G., Riccardi, D., Lombardi, M., Butters, R., Kifor, O., Sun, A., Hediger, M. A., Lytton, J., & Hebert, S. C. (1993). Cloning and characterization of an extracellular Ca^{2+}-sensing receptor from bovine parathyroid. Nature, 366, 575–580. https://doi.org/10.1038/366575a0

Cao, L., Hunt, C. J., Lin, S., Meyer, A. S., Li, Q., & Lametsch, R. (2023). Elucidation of the molecular mechanism of bovine milk γ-glutamyltransferase-catalyzed formation of γ-glutamyl-valyl-glycine. Journal of Agricultural and Food Chemistry, 71, 2455–2463. https://doi.org/10.1021/acs.jafc.2c08386

Chang, J., Feng, T., Zhuang, H., Song, S., Sun, M., Yao, L., Wang, H., Hou, F., Xiong, J., Li, F., et al. (2022). Taste mechanism of kokumi peptides from yeast extracts revealed by molecular docking and molecular dynamics simulation. Journal of Future Foods, 2, 358–364. https://doi.org/10.1016/j.jfutfo.2022.08.007

Chen, X., Gabitto, M., Peng, Y., Ryba, N. J. P., & Zuker, C. S. (2011). A gustotopic map of taste qualities in the mammalian brain. Science, 333, 1262–1266. https://doi.org/10.1126/science.1204076

Chen, X., & Li, H. (2017). ArControl: An Arduino-based comprehensive behavioral platform with real-time performance. Frontiers in Behavioral Neuroscience, 11, 244. https://doi.org/10.3389/fnbeh.2017.00244

Chun, J.-Y., Kim, B.-S., Lee, J.-G., Cho, H.-Y., Min, S.-G., & Choi, M.-J. (2014). Effect of NaCl/monosodium glutamate (MSG) mixture on the sensorial properties and quality characteristics of model meat products. Korean Journal for Food Science of Animal Resources, 34, 576–581. https://doi.org/10.5851/kosfa.2014.34.5.576

Cui, Z., Wu, B., Blank, I., Yu, Y., Gu, J., Zhou, T., Zhang, Y., Wang, W., & Liu, Y. (2023). TastePeptides-EEG: An ensemble model for umami taste evaluation based on electroencephalogram and machine learning. Journal of Agricultural and Food Chemistry, 71, 13430–13439. https://doi.org/10.1021/acs.jafc.3c04611

Ebenso, E. E., Verma, C., Olasunkanmi, L. O., Akpan, E. D., Verma, D. K., Lgaz, H., Guo, L., Kaya, S., & Quraishi, M. A. (2021). Molecular modelling of compounds used for corrosion inhibition studies: A review. Physical Chemistry Chemical Physics, 23, 19987–20027. https://doi.org/10.1039/D1CP00244A

Feng, T., Ma, C., Chen, S., Zhuang, H., Song, S., Sun, M., Yao, L., Wang, H., Liu, Q., & Yu, C. (2024). Exploring novel kokumi peptides in Agaricus bisporus: Selection, identification, and tasting mechanism investigation through sensory evaluation and computer simulation analysis. Food & Function, 15, 2879–2894. https://doi.org/10.1039/D3FO05406C

Feng, X., Wang, R., Lu, J., Du, Q., Cai, K., Zhang, B., & Xu, B. (2024). Taste properties and mechanism of umami peptides from fermented goose bones based on molecular docking and molecular dynamics simulation using umami receptor T1R1/T1R3. Food Chemistry, 443, 138570. https://doi.org/10.1016/j.foodchem.2024.138570

Glabasnia, A., & Hofmann, T. (2006). Sensory-directed identification of taste-active ellagitannins in American oak (Quercus alba L.) and European oak (Quercus robur L.) and quantitative analysis in bourbon whiskey and oak-matured red wines. Journal of Agricultural and Food Chemistry, 54, 3380–3390. https://doi.org/10.1021/jf052617b

Guo, Y., Gao, S., Jiang, Z., Huang, J., He, X., Jin, R., Sun, S., Guo, F., Gong, Y., & Sun, X. (2021). Calcium-sensing receptor (CaSR) agonist R568 inhibits small intestinal motility of mice through neural and non-neural mechanisms. Food & Function, 12, 11926–11937. https://doi.org/10.1039/D1FO01988K

Hao, X., Chen, J., Luo, Z., He, H., Yu, H., Ma, L., Ma, S., Zhu, T., Liu, D., & Zhu, Z. (2011). TRPV1 activation prevents high-salt diet-induced nocturnal hypertension in mice. Pflügers Archiv—European Journal of Physiology, 461, 345–353. https://doi.org/10.1007/s00424-011-0921-x

He, Y., Liu, K., Yu, X., Yang, H., & Han, W. (2024). Building a kokumi database and machine learning-based prediction: A systematic computational study on kokumi analysis. Journal of Chemical Information and Modeling. https://doi.org/10.1021/acs.jcim.3c01728

Hendy, G. N., Canaff, L., & Cole, D. E. C. (2013). The CASR gene: Alternative splicing and transcriptional control, and calcium-sensing receptor (CaSR) protein: Structure and

ligand binding sites. Best Practice & Research Clinical Endocrinology & Metabolism, 27, 285–301. https://doi.org/10.1016/j.beem.2013.02.009

Hollebrands, B., Thong, G., & Janssen, H. (2026). Integrated targeted and untargeted analysis of polar peptides in foods using hydrophilic interaction liquid chromatography-data-independent acquisition-mass spectrometry. Analytical and Bioanalytical Chemistry, 418, 3013–3024. https://doi.org/10.1007/s00216-026-06322-7

Kobayashi, Y., Habara, M., Ikezazki, H., Chen, R., Naito, Y., & Toko, K. (2010). Advanced taste sensors based on artificial lipids with global selectivity to basic taste qualities and high correlation to sensory scores. Sensors, 10, 3411–3443. https://doi.org/10.3390/s100403411

Kurihara, K., & Kashiwayanagi, M. (2000). Physiological studies on umami taste. Journal of Nutrition, 130, 931S–934S. https://doi.org/10.1093/jn/130.4.931S

Kuroda, M. (2022). Increases in the pungency of allyl isothiocyanate by CaSR agonists, glutathione and γ-glutamyl-valyl-glycine. SSRN. https://doi.org/10.2139/ssrn.4111682

Lao, H., Chang, J., Zhuang, H., Song, S., Sun, M., Yao, L., Wang, H., Liu, Q., Xiong, J., Li, P., et al. (2024). Novel kokumi peptides from yeast extract and their taste mechanism via an in silico study. Food & Function, 15, 2459–2473. https://doi.org/10.1039/D3FO04487D

Li, H., Feng, X., Liu, Z., Wang, W., Tian, L., Xu, D., Chitrakar, B., Cui, Z., Hu, L., & Mo, H. (2025). The influence of different flavor peptides on brain perception via scalp electroencephalogram and development of a taste model. Food Chemistry, 465, 141953. https://doi.org/10.1016/j.foodchem.2024.141953

Li, J., Yi, H.-B., Wang, P., Wang, S.-N., Liu, H., & Zhang, N. (2024). Current advances in the salt reduction properties of kokumi γ-glutamyl peptides: A review. Food Reviews International, 1–21. https://doi.org/10.1080/87559129.2024.2412866

Li, Q., Zhang, L., & Lametsch, R. (2022). Current progress in kokumi-active peptides, evaluation and preparation methods: A review. Critical Reviews in Food Science and Nutrition, 62, 1230–1241. https://doi.org/10.1080/10408398.2020.1837726

Li, Y., Bi, J., Lin, Z., Yang, Z., Gao, Y., Ping, C., & Chen, Z. (2023). Mining of kokumi peptides in chicken broth with peptidomics. International Journal of Gastronomy and Food Science, 32, 100693. https://doi.org/10.1016/j.ijgfs.2023.100693

Liu, J., Song, H., Liu, Y., Li, P., Yao, J., & Xiong, J. (2015). Discovery of kokumi peptide from yeast extract by LC-Q-TOF-MS/MS and sensomics approach. Journal of the Science of Food and Agriculture, 95, 3183–3194. https://doi.org/10.1002/jsfa.7058

Maruyama, Y., Yasuda, R., Kuroda, M., & Eto, Y. (2012). Kokumi substances, enhancers of basic tastes, induce responses in calcium-sensing receptor-expressing taste cells. PLoS ONE, 7, e34489. https://doi.org/10.1371/journal.pone.0034489

Nishimura, T., & Kuroda, M. (Eds.). (2019). Koku in food science and physiology: Recent research on a key concept in palatability. Springer. ISBN 978-981-13-8452-3

Ohsu, T., Amino, Y., Nagasaki, H., Yamanaka, T., Takeshita, S., Hatanaka, T., Maruyama, Y., Miyamura, N., & Eto, Y. (2010). Involvement of the calcium-sensing receptor in human taste perception. Journal of Biological Chemistry, 285, 1016–1022. https://doi.org/10.1074/jbc.M109.029165

Park, G. Y., Lee, G., Yoon, J., Han, J., Choi, P., Kim, M., Lee, S., Park, C., Wu, Z., Li, Y., et al. (2025). Glia-like taste cells mediate an intercellular mode of peripheral sweet adaptation. Cell, 188, 141–156.e16. https://doi.org/10.1016/j.cell.2024.10.041

Perenzoni, D., Dellafiora, L., Perugino, F., Vrhovsek, U., Piombino, P., Pittari, E., Guzzon, R., Moio, L., Galaverna, G., & Mattivi, F. (2024). Exploring putative kokumi oligopeptides in classic sparkling wines with a UHPLC-ESI-MS/MS targeted protocol. Journal of Agricultural and Food Chemistry, 72, 26189–26208. https://doi.org/10.1021/acs.jafc.4c08213

Pluskal, T., & Weng, J.-K. (2018). Natural product modulators of human sensations and mood: Molecular mechanisms and therapeutic potential. Chemical Society Reviews, 47, 1592–1637. https://doi.org/10.1039/C7CS00411G

Rentzsch, R., & Renard, B. Y. (2015). Docking small peptides remains a great challenge: An assessment using AutoDock Vina. Briefings in Bioinformatics, 16, 1045–1056. https://doi.org/10.1093/bib/bbv008

Shan, Y., Pu, D., Cao, B., Shi, Y., Li, P., Xiong, J., Li, K., Sun, B., & Zhang, Y. (2024). Elucidating salt-reduction mechanisms of aroma-active compounds from yeast extracts through sensomics approaches and electroencephalography. Food Chemistry: X, 22, 101339. https://doi.org/10.1016/j.fochx.2024.101339

Tahara, Y., & Toko, K. (2013). Electronic tongues—A review. IEEE Sensors Journal, 13, 3001–3011. https://doi.org/10.1109/JSEN.2013.2263125

Ueda, Y., Sakaguchi, M., Hirayama, K., Miyajima, R., & Kimizuka, A. (1990). Characteristic flavor constituents in water extract of garlic. Agricultural and Biological Chemistry, 54, 163–169. https://doi.org/10.1080/00021369.1990.10869909

Ueda, Y., Yonemitsu, M., Tsubuku, T., Sakaguchi, M., & Miyajima, R. (1997). Flavor characteristics of glutathione in raw and cooked foodstuffs. Bioscience, Biotechnology, and Biochemistry, 61, 1977–1980. https://doi.org/10.1271/bbb.61.1977

Wang, Y., Xiao, T., Zhang, Z., & Feng, X. (2022). Extraction and concentration of glutathione from yeast by membranes. Canadian Journal of Chemical Engineering, 100, S195–S204. https://doi.org/10.1002/cjce.24084

Wang, Z., Sun, H., Yao, X., Li, D., Xu, L., Li, Y., Tian, S., & Hou, T. (2016). Comprehensive evaluation of ten docking programs on a diverse set of protein–ligand

complexes: The prediction accuracy of sampling power and scoring power. Physical Chemistry Chemical Physics, 18, 12964–12975. https://doi.org/10.1039/C6CP01555G

Xia, X., Fu, Y., Ma, L., Zhu, H., Yu, Y., Dai, H., Han, J., Liu, X., Liu, Z., & Zhang, Y. (2022). Protein hydrolysates from Pleurotus geesteranus modified by Bacillus amyloliquefaciens γ-glutamyl transpeptidase exhibit a remarkable taste-enhancing effect. Journal of Agricultural and Food Chemistry, 70, 12143–12155. https://doi.org/10.1021/acs.jafc.2c03941

Xu, X., You, M., Song, H., Gong, L., & Pan, W. (2018). Investigation of umami and kokumi taste-active components in bovine bone marrow extract produced during enzymatic hydrolysis and Maillard reaction. International Journal of Food Science & Technology, 53, 2465–2481. https://doi.org/10.1111/ijfs.13893

Yamaguchi, H., Kitajima, S., Suzuki, H., Suzuki, S., Nishikawa, K., Kamegawa, A., Fujiyoshi, Y., Takahashi, K., Tagami, U., Maruyama, Y., et al. (2025). Cryo-EM structure of the calcium-sensing receptor complexed with the kokumi substance γ-glutamyl-valyl-glycine. Scientific Reports, 15, 3894. https://doi.org/10.1038/s41598-025-87999-1

Yamamoto, T., & Mizuta, H. (2022). Supplementation effects of a kokumi substance, γ-Glu-Val-Gly, on the ingestion of basic taste solutions in rats. Chemical Senses, 47, bjac008. https://doi.org/10.1093/chemse/bjac008

Yamamoto, T., Watanabe, U., Fujimoto, M., & Sako, N. (2009). Taste preference and nerve response to 5′-inosine monophosphate are enhanced by glutathione in mice. Chemical Senses, 34, 809–818. https://doi.org/10.1093/chemse/bjp070

Yamamoto, T., Ueji, K., Mizuta, H., Inui-Yamamoto, C., Kumamoto, N., Shibata, Y., & Ugawa, S. (2025). GPRC6A as a novel kokumi receptor responsible for enhanced taste preferences by ornithine. eLife, 13, RP101629. https://doi.org/10.7554/eLife.101629

Yang, C., Du, Y., Wang, G., Liu, J., Tan, J., Tang, S., Liu, Y., Pan, H., & Liao, G. (2025). Discovery and mechanistic profiling of novel kokumi peptides from Wuding chicken soup. Food Chemistry: X, 31, 103171. https://doi.org/10.1016/j.fochx.2025.103171

Yi, H., Li, J., Wang, P., Wang, S., Guo, X., Zhu, D., Liu, H., & Zhang, N. (2025). Synthesis of umami-, salty-, and kokumi-enhancing γ-glutamyl peptides from soy protein isolate hydrolysate and their taste mechanism via an in silico study. Food and Bioprocess Technology, 18, 7544–7560. https://doi.org/10.1007/s11947-025-03894-7

Zhang, J., Zhao, M., Su, G., & Lin, L. (2019). Identification and taste characteristics of novel umami and umami-enhancing peptides separated from peanut protein isolate hydrolysate by consecutive chromatography and UPLC–ESI–QTOF–MS/MS. Food Chemistry, 278, 674–682. https://doi.org/10.1016/j.foodchem.2018.11.114

Zhao, J., Liao, S., Bi, X., Zhao, J., Liu, P., Ding, W., Che, Z., Wang, Q., & Lin, H. (2022). Isolation, identification and characterization of taste peptides from fermented

broad bean paste. Food & Function, 13, 8730–8740. https://doi.org/10.1039/D2FO01389D

Zhu, J., Xia, X., Zhang, F., Song, S., Cui, H., Hayat, K., Zhang, Q., Zhang, X., & Ho, C.-T. (2023). Taste characteristic and the mechanism of light-colored Maillard reaction products derived from gluten hydrolysate. Food Bioscience, 52, 102394. https://doi.org/10.1016/j.fbio.2023.102394

Figure legends

Fig. 1. Identification and computational screening of kokumi-active peptides from yeast extract.

(A) Schematic workflow for yeast-extract sample preparation, including desalting and purification followed by liquid chromatography–tandem mass spectrometry (LC–MS/MS) analysis. (B) Representative LC–MS/MS total ion chromatogram of the desalted and purified yeast-extract fraction. (C) Integrated peptide-identification and molecular-docking workflow. A total of 8,474 peptides were identified, of which 5,917 were unmodified. After filtering for peptides containing no more than 14 amino acids, 4,772 candidate peptides were retained for ligand modeling and docking analysis. The crystal structure of the human calcium-sensing receptor (CaSR; PDB ID: 5K5S) was prepared as the docking receptor, and the candidate peptides were modeled as ligands. Following molecular docking and generation of peptide–CaSR complexes, 2,608 successfully docked complexes were retained for binding-site analysis and subsequent screening. Arrows indicate the sequential computational and analytical procedures. LC–MS/MS, liquid chromatography–tandem mass spectrometry; CaSR, calcium-sensing receptor; PDB, Protein Data Bank.

Fig. 2. Computational analysis of peptide–CaSR interactions and structural validation of RSQPVGV.

(A) Distribution of candidate peptides according to peptide length. Pink bars indicate the number of peptides at each length, whereas the green line indicates the corresponding molecular-docking success rate. The left and right axes represent peptide number and docking success rate, respectively. (B) Frequencies of interaction types identified between the successfully docked peptides and individual CaSR residues.

Stacked bars represent the total interaction count for each residue, with colors indicating hydrophobic interactions, hydrogen bonds, salt bridges, π-stacking, and π-cation interactions. (C) Spatial distribution of peptide-binding sites on the CaSR structure. The enlarged view shows the docking region and the distribution of interacting peptides, with colors representing the number of peptide complexes associated with each binding-site region according to the indicated scale. (D) Distribution of successfully docked peptides according to peptide length. The pie chart summarizes the number of peptides in each length category, and the accompanying bar chart shows the distribution of peptides according to the docking-score interval (*S*). Numbers in parentheses indicate the number of peptides in each category. (E) Representative tandem mass spectrum confirming the sequence of the selected peptide RSQPVGV. The annotated fragment ions support peptide-sequence assignment by matching the observed product ions with the expected sequence-specific fragmentation pattern. CaSR, calcium-sensing receptor; MS/MS, tandem mass spectrometry.

Fig. 3. Molecular docking and molecular dynamics (MD) simulation analyses of GSH–CaSR and RSQPVGV–CaSR complexes.

(A,B) Representative docking poses of GSH (A) and RSQPVGV (B) bound to the calcium-sensing receptor (CaSR). The predicted binding energies were −6.031 and −9.929 kcal/mol for GSH and RSQPVGV, respectively. Residues involved in ligand binding are labeled. Solid blue lines indicate hydrogen bonds, yellow dotted lines indicate salt bridges, and gray dashed lines indicate hydrophobic interactions. (C,D) Time-dependent root-mean-square deviation (RMSD) of the ligand–protein complexes (C) and CaSR backbone atoms (D) during 100 ns of MD simulation. GSH and RSQPVGV are represented by orange and yellow traces, respectively. (E) Number of

hydrogen bonds formed between each ligand and CaSR throughout the simulation; black and red traces represent GSH and RSQPVGV, respectively. (F) Solvent-accessible surface area (SASA) of the ligand–CaSR complexes during the simulation. Dark- and light-blue traces represent the GSH and RSQPVGV complexes, respectively. (G,H) Free-energy landscapes for the GSH–CaSR (G) and RSQPVGV–CaSR (H) complexes, plotted as a function of the radius of gyration (R_g) and backbone RMSD. The color scale represents relative free energy in kcal/mol, with blue and purple regions indicating lower-energy conformational states and red regions indicating higher-energy states. CaSR, calcium-sensing receptor; GSH, glutathione; RMSD, root-mean-square deviation; SASA, solvent-accessible surface area; MD, molecular dynamics.

Fig. 4. Surface plasmon resonance analysis of the interactions of GSH and RSQPVGV with the calcium-sensing receptor.

(A) Proposed mechanism of action of kokumi peptides. Kokumi peptides released in the oral cavity interact with CaSR on taste-bud cells and enhance taste perception, whereas the CaSR antagonist NPS-2143 blocks this interaction. (B) Schematic representation of the surface plasmon resonance (SPR) assay. CaSR, GSH, or RSQPVGV was immobilized on the CM5 sensor chip, and the indicated flowing molecules were injected over the immobilized ligand. The experimental configurations were as follows: CaSR immobilized with GSH as the analyte (C,D); CaSR immobilized with RSQPVGV as the analyte (E,F); GSH immobilized with NPS-2143 as the analyte (G); and RSQPVGV immobilized with NPS-2143 as the analyte (H). (C,E) Representative SPR sensorgrams showing concentration-dependent responses to GSH and RSQPVGV, respectively. The analyte concentrations ranged from 1.56 to 100 μM, as indicated in the legends. (D,F) Corresponding concentration–response curves for

GSH–CaSR and RSQPVGV–CaSR binding. The estimated binding parameters were 1.05×10^{-4} M for GSH and 1.91×10^{-5} M for RSQPVGV. (G,H) SPR responses obtained by injecting NPS-2143 over immobilized GSH and RSQPVGV, respectively, at the indicated concentrations. RU, response units; SPR, surface plasmon resonance; CaSR, calcium-sensing receptor; GSH, glutathione.

Fig. 5. Sensory evaluation and electronic-tongue analysis of kokumi peptide-enhanced monosodium glutamate solutions.

(A) Schematic overview of the human sensory-evaluation procedure. Test solutions were prepared, presented to participants for tasting, and evaluated using a standardized sensory questionnaire. (B) Radar plot comparing the perceived intensities of the basic taste modalities and kokumi among MNS, MNS supplemented with 0.1% GSH, and MNS supplemented with 0.1% RSQPVGV. (C) Quantitative sensory scores for salty, umami, and kokumi perceptions. The addition of GSH or RSQPVGV increased the perceived intensities of these attributes relative to MNS alone, with RSQPVGV producing the strongest kokumi response. Data are presented as means±SD; asterisks indicate statistically significant differences between the indicated groups. (D) Schematic workflow for electronic-tongue analysis. The test solutions were loaded into the sensor system, and the resulting sensor responses were acquired and processed to generate taste-profile data. (E) Richness values determined by electronic-tongue analysis for MNS, MNS+0.1% GSH, and MNS+0.1% RSQPVGV. Both peptide-containing solutions showed greater richness than MNS alone, with the RSQPVGV-supplemented solution exhibiting the highest value. Bars represent means±SD. Statistical significance is indicated as follows: *$p<0.01$, **$p<0.01$ and ***$p<0.001$.

MNS, monosodium glutamate-containing solution; GSH, glutathione; RSQPVGV, kokumi peptide.

Fig. 6. Effects of GSH and RSQPVGV on taste preference and ingestive behavior in mice.

(A) Representative image and schematic of the two-bottle licking assay used to assess solution preference in mice. (B) Preference scores for different dilution ratios of MNS, defined as a solution containing 1% MSG and 0.3% NaCl. (C,D) Preference scores for solutions supplemented with 0.1% GSH (C) or 0.1% RSQPVGV (D), compared with the indicated control solutions. The dashed horizontal line represents a preference score of 0.5, corresponding to no preference between the test and control solutions. (E,F) Cumulative lick counts during 1,800 s of access to 0.6% MSG, 0.6% MSG supplemented with 0.1% GSH (E) or 0.1% RSQPVGV (F), and the corresponding solutions additionally containing 0.005% NPS-2143. Shaded areas represent the variability of the measurements. (G,H) Total lick counts during the 1,800-s test period for the GSH-containing (G) and RSQPVGV-containing (H) solutions. Each point represents an individual mouse, and bars indicate group means. Statistical significance was assessed using the indicated comparisons; ns, not significant; *$p<0.05$, **$p<0.01$, ***$p<0.001$, and ****$p<0.0001$. MNS, monosodium glutamate-containing solution; MSG, monosodium glutamate; GSH, glutathione; RSQPVGV, kokumi peptide; NPS-2143, calcium-sensing receptor antagonist.

Fig. 7. Gustatory-cortex calcium responses to RSQPVGV- and MSG-containing solutions in mice.

(A) Schematic of the behavioral calcium-imaging experiment. Mice were presented with distilled water, 0.1% RSQPVGV, 0.6% MSG, or 0.6% MSG supplemented with 0.1% RSQPVGV, and licking behavior was monitored while optical signals were recorded. (B) Schematic of the fiber-photometry recording setup, including the implanted optical fiber, LED excitation source, lens, CMOS detector, amplifier, and data-acquisition system. Red arrows indicate representative lick-related optical events; the scale bar denotes a 10-s interval and the fluorescence signal is expressed as the relative change in fluorescence (ΔF/F). (C) Schematic of viral delivery and fiber placement in the gustatory cortex. AAV2/9-mCaMKIIα-GCaMP6s-WPRE-pA was used to express the calcium indicator GCaMP6s in CaMKIIα-positive neurons. The representative fluorescence image shows GCaMP6s expression and the recording region; scale bar, as indicated. (D-F) Representative calcium-signal heat maps and peri-lick traces aligned to the onset of a lick burst (time 0, indicated by the dashed vertical line) during presentation of 0.1% RSQPVGV (D), 0.6% MSG (E), or 0.6% MSG supplemented with 0.1% RSQPVGV (F). Each heat map displays fluorescence responses across individual trials or recording events, and the traces show the mean response with the corresponding shaded variability. The mixed MSG-RSQPVGV solution elicited a larger and more sustained gustatory-cortex response than either component alone. (G) Definition of the area-under-the-curve (AUC) analysis window used to quantify lick-associated calcium responses. The shaded region represents the post-lick interval included in the analysis. (H) Quantification of the AUC of ΔF/F0 responses evoked by the four solutions. Bars represent means±SD. Statistical significance is indicated as follows: *$p<0.05$; ns, not significant. MSG, monosodium glutamate; RSQPVGV, peptide; GCaMP6s, genetically encoded calcium indicator; AAV, adeno-associated virus; AUC, area under the curve.

Fig. 8. Electrophysiological and cortical responses to RSQPVGV, MSG, and their combination in human participants.

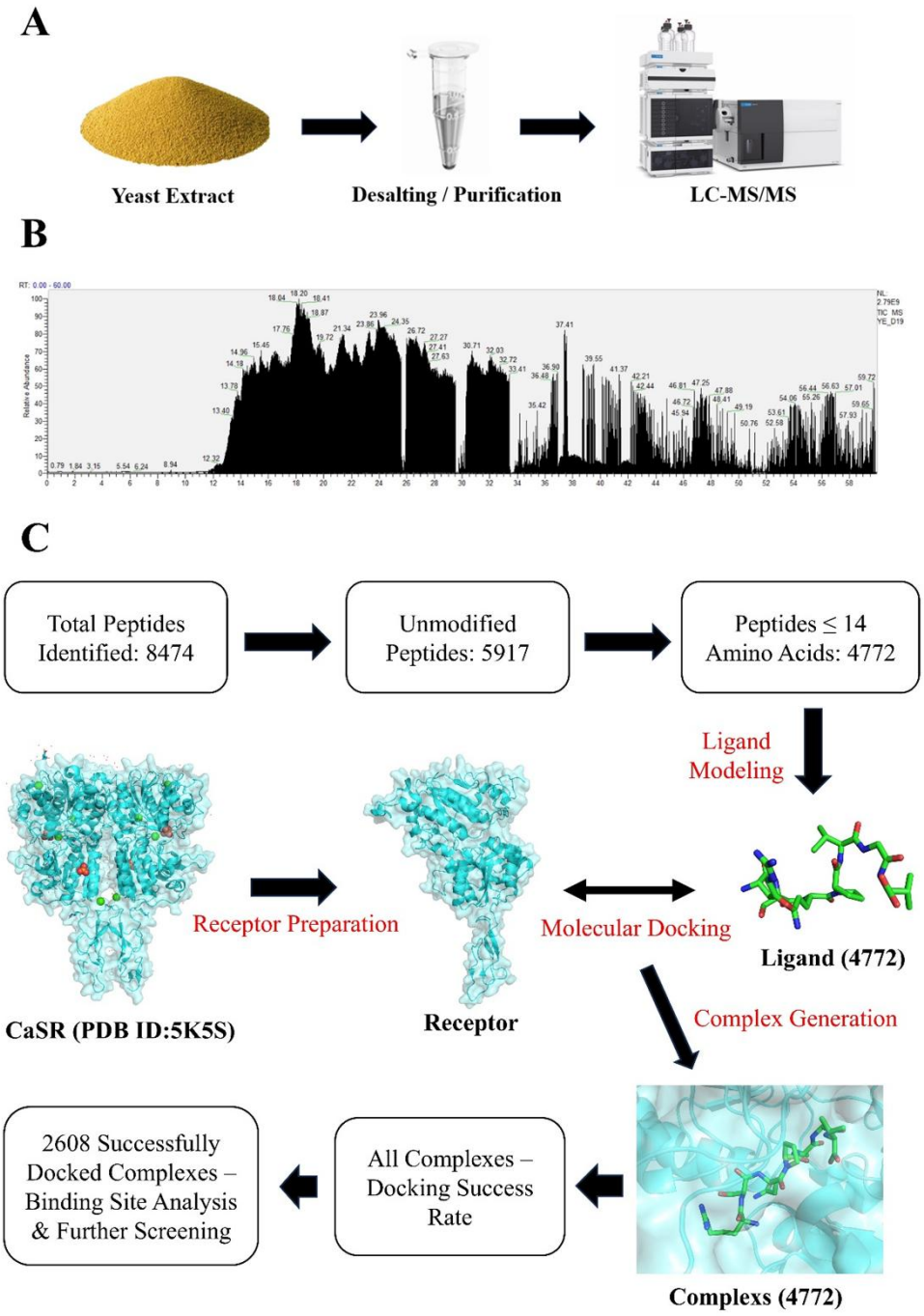
(A) Schematic of the experimental protocol. Participants received water, 0.1% RSQPVGV, 0.6% MSG, or a mixture of 0.1% RSQPVGV and 0.6% MSG through an oral delivery system while electroencephalographic (EEG) activity was recorded. Following a 5-min stable-baseline period, 200 μL of each sample was delivered, held in the mouth for 10 s, expectorated, and followed by an oral rinse. The procedure was repeated 10 times sequentially for each sample, with a 5-min baseline-restoration period between conditions. (B) Grand-average event-related potential (ERP) waveforms elicited by the four solutions. The N1, N2, and P300 components are indicated, and the dashed vertical line marks the stimulus-delivery reference point. (C–E) Quantification of ERP component amplitudes for N1 (C), N2 (D), and P300 (E). Bars represent the mean amplitude±SD for water, RSQPVGV, MSG, and RSQPVGV+MSG. Statistical comparisons are indicated by horizontal brackets; ns, not significant; $*p<0.05$; $**p<0.01$. (F) Time–frequency representations of EEG activity following sample delivery. Color indicates the event-related spectral perturbation, expressed as the change in decibels (dB) relative to baseline. Beta-band event-related synchronization (ERS) and alpha-band event-related desynchronization (ERD) are indicated. The dashed lines denote the analysis boundaries or stimulus-alignment time points. (G) Scalp topographies of beta-band power responses evoked by the four solutions. The color scale represents normalized beta-band power, with warmer and cooler colors indicating higher and lower activity, respectively. (H) Quantification of beta-band power. The combined RSQPVGV+MSG solution produced the strongest beta-band response, whereas water and RSQPVGV alone elicited comparatively smaller responses. Bars

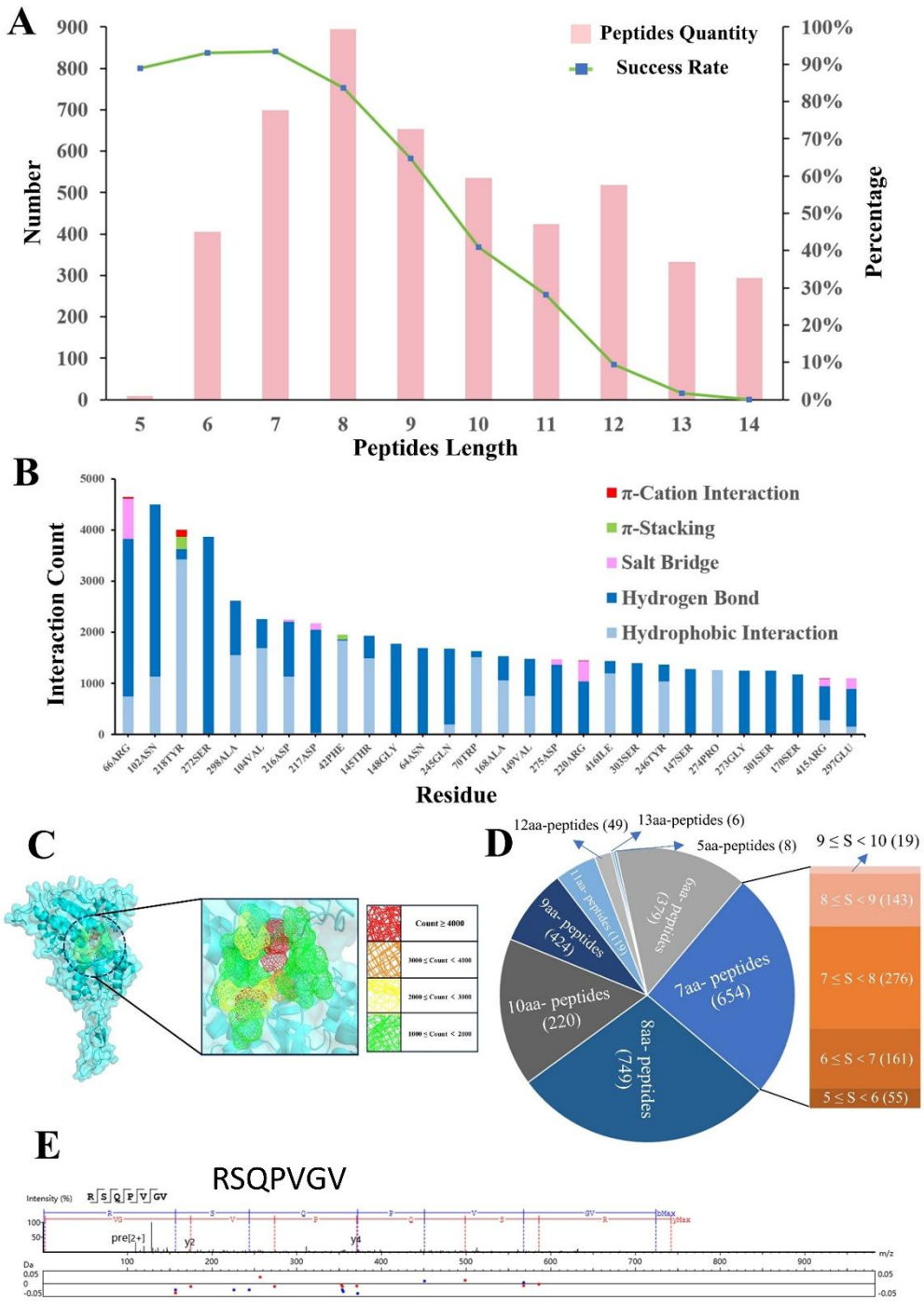
represent means±SD; ns, not significant; *p<0.05; ****p<0.0001. (I) Source-localized cortical activity associated with sample presentation, highlighting responses in the orbitofrontal cortex (OFC) and insular cortex. Color indicates estimated cortical current density. (J) Quantification of OFC current density for the four treatment conditions. The RSQPVGV+MSG combination elicited the greatest OFC response. Bars represent means±SD; ns, not significant; *p<0.05; ****p<0.0001. MSG, monosodium glutamate; ERP, event-related potential; EEG, electroencephalography; ERD, event-related desynchronization; ERS, event-related synchronization; OFC, orbitofrontal cortex.

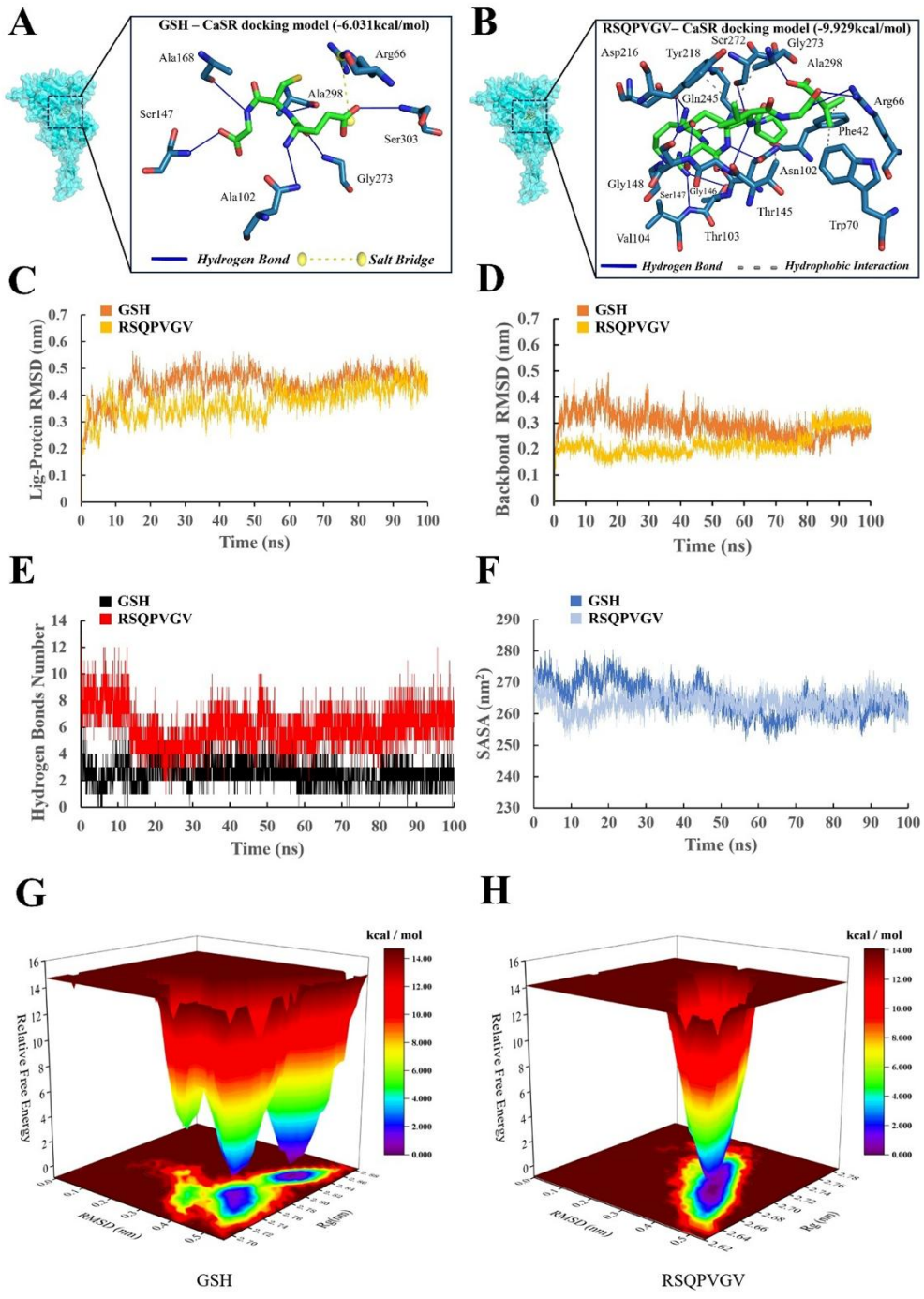
Table 1. Descriptive sensory evaluation and taste thresholds of kokumi peptides in MNS.

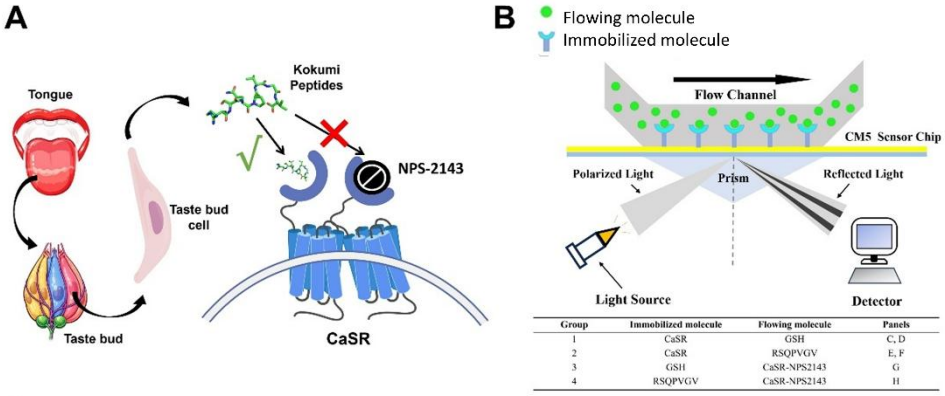
Sample	Sensory characteristics	Threshold (mmol/L)	Threshold (g/L)
MNS	Slight salty taste, slight umami taste, almost no kokumi sensation	-	-
MNS+GSH	Strong umami taste, moderate salty taste, moderate kokumi sensation	0.31	9.57×10^{-2}

MNS+RSQPVGV	**Strong umami taste, moderate salty taste, strong kokumi sensation**	**0.37**	**2.72×10^{-1}**

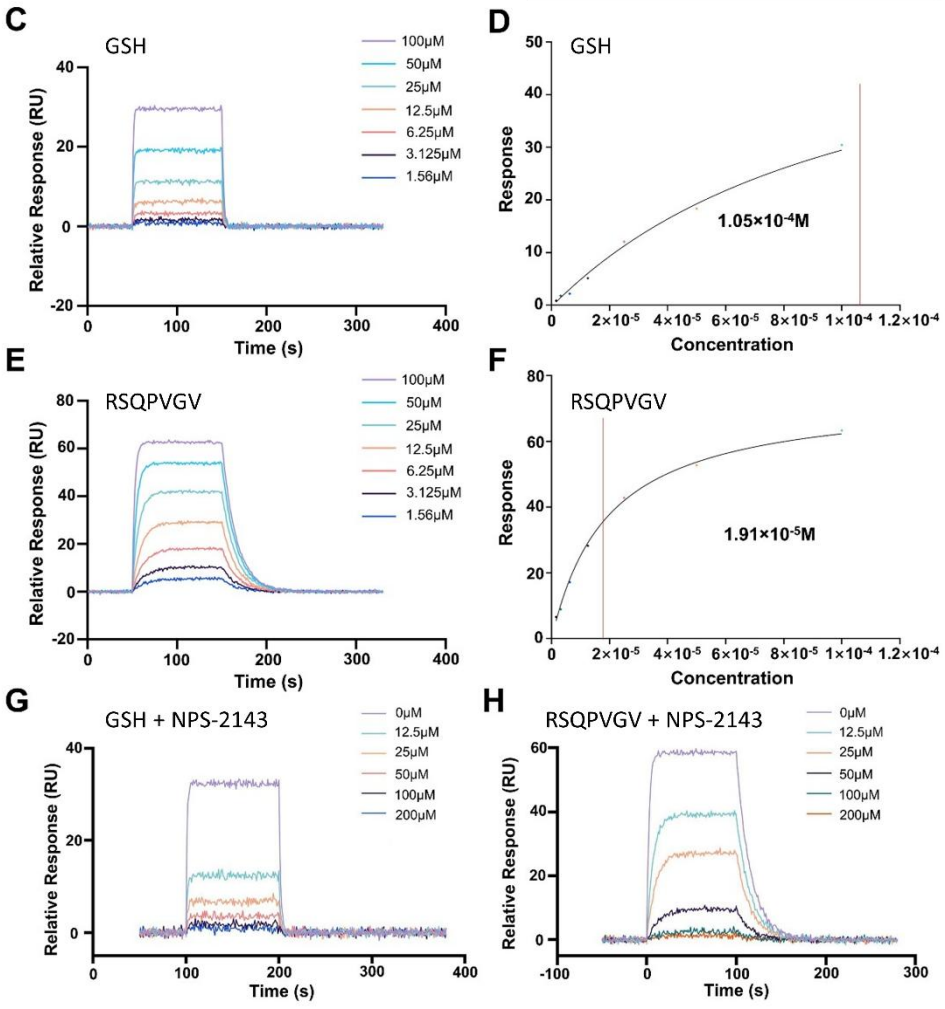

A
Yeast Extract
Desalting / Purification
LC-MS/MS
B
C
Total Peptides Identified: 8474
Unmodified Peptides: 5917
Peptides ≤ 14 Amino Acids: 4772
Ligand Modeling
Ligand (4772)
Molecular Docking
Receptor Preparation
CaSR (PDB ID:5K5S)
Receptor
Complex Generation
Complexs (4772)
All Complexes – Docking Success Rate
2608 Successfully Docked Complexes – Binding Site Analysis & Further Screening

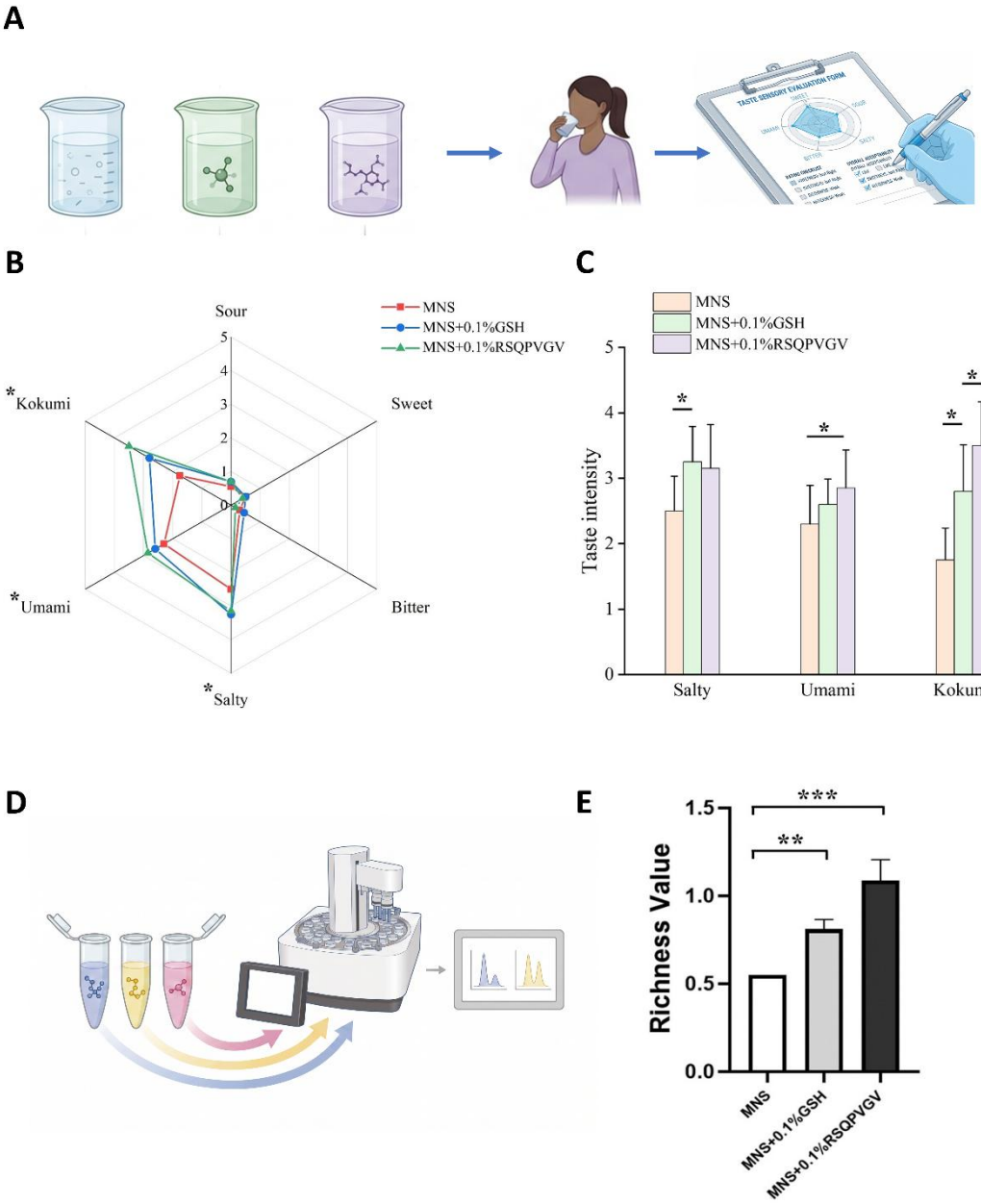

A
Peptides Quantity
Success Rate
Number
Percentage
Peptides Length
B
π-Cation Interaction
π-Stacking
Salt Bridge
Hydrogen Bond
Hydrophobic Interaction
Interaction Count
Residue
C
Count ≥ 4000
3000 ≤ Count < 4000
2000 ≤ Count < 3000
1000 ≤ Count < 2000
D
12aa-peptides (49)
13aa-peptides (6)
5aa-peptides (8)
9 ≤ S < 10 (19)
8 ≤ S < 9 (143)
7 ≤ S < 8 (276)
6 ≤ S < 7 (161)
5 ≤ S < 6 (55)
7aa- peptides (654)
8aa- peptides (749)
10aa- peptides (220)
9aa- peptides (424)
11aa- peptides (119)
6aa- Peptides (379)
E
RSQPVGV
Intensity (%)
pre[2+]
y2
y4
m/z
Da

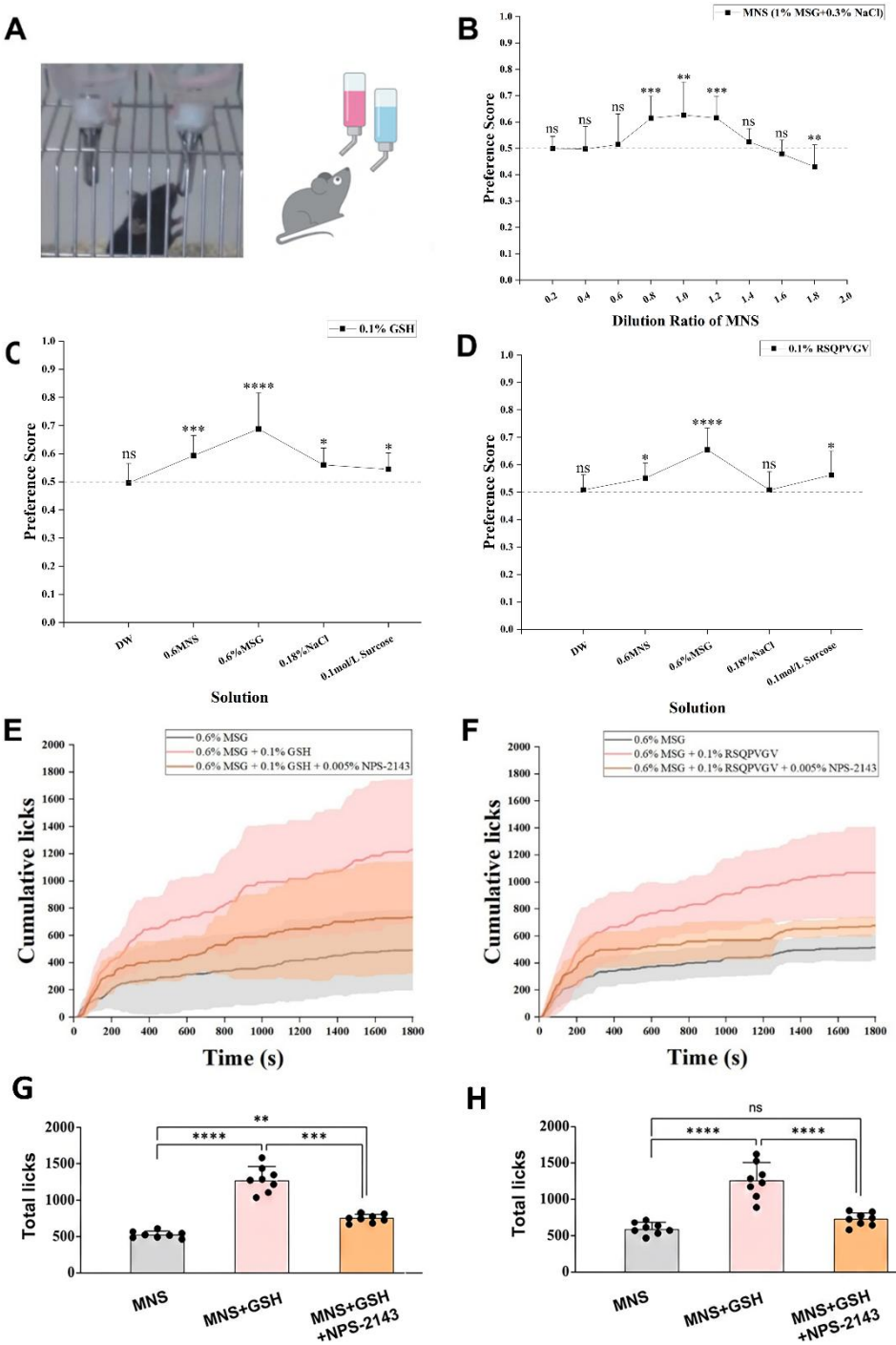

A
GSH – CaSR docking model (-6.031kcal/mol)
Ala168
Arg66
Ala298
Ser147
Ser303
Gly273
Ala102
Hydrogen Bond
Salt Bridge
B
RSQPVGV– CaSR docking model (-9.929kcal/mol)
Asp216
Tyr218
Ser272
Gly273
Ala298
Gln245
Arg66
Phe42
Asn102
Gly148
Ser147
Gly146
Thr145
Trp70
Val104
Thr103
Hydrogen Bond
Hydrophobic Interaction
C
GSH
RSQPVGV
Lig-Protein RMSD (nm)
Time (ns)
D
GSH
RSQPVGV
Backbond RMSD (nm)
Time (ns)
E
GSH
RSQPVGV
Hydrogen Bonds Number
Time (ns)
F
GSH
RSQPVGV
SASA (nm²)
Time (ns)
G
kcal / mol
Relative Free Energy
RMSD (nm)
Rg (nm)
GSH
H
kcal / mol
Relative Free Energy
RMSD (nm)
Rg (nm)
RSQPVGV

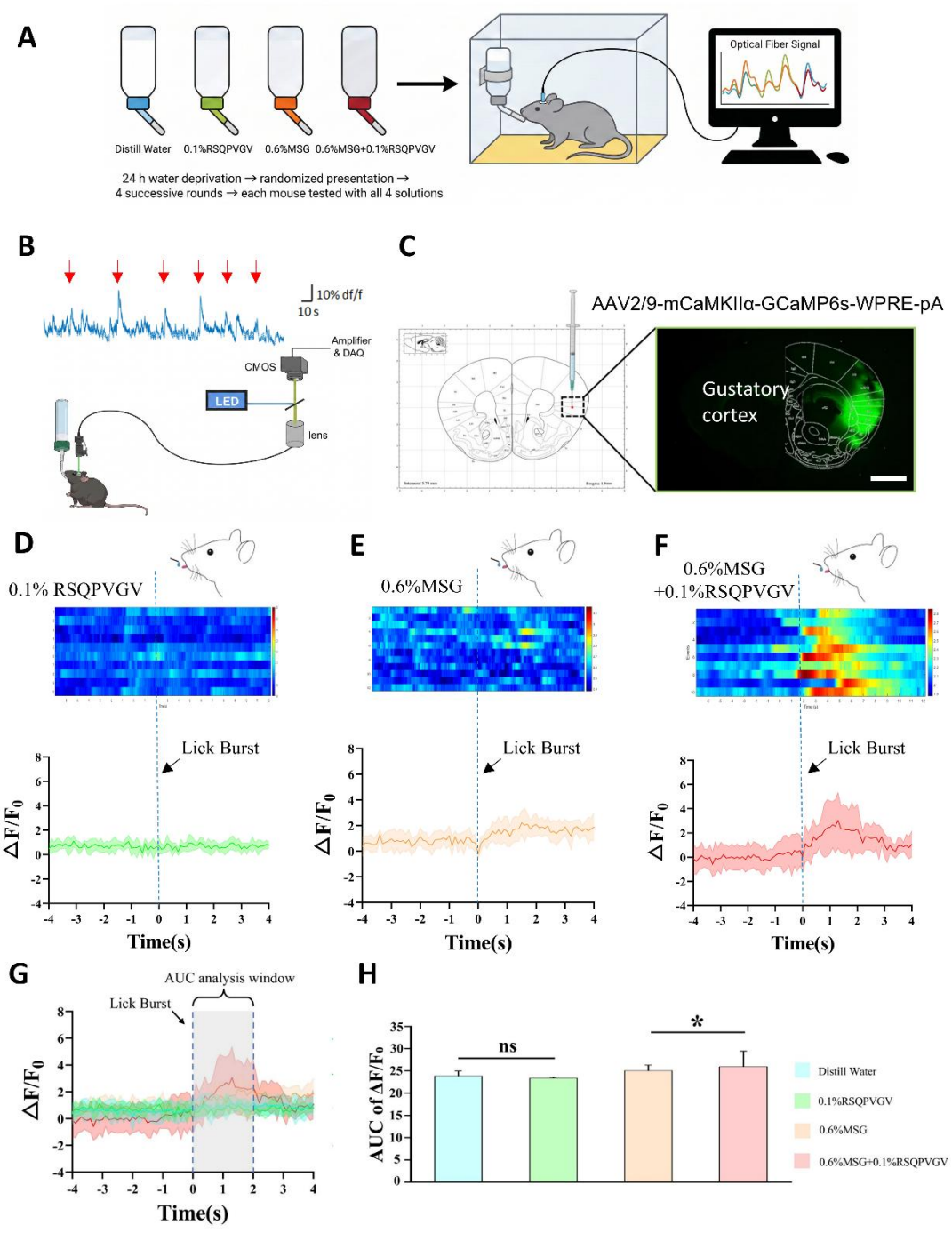


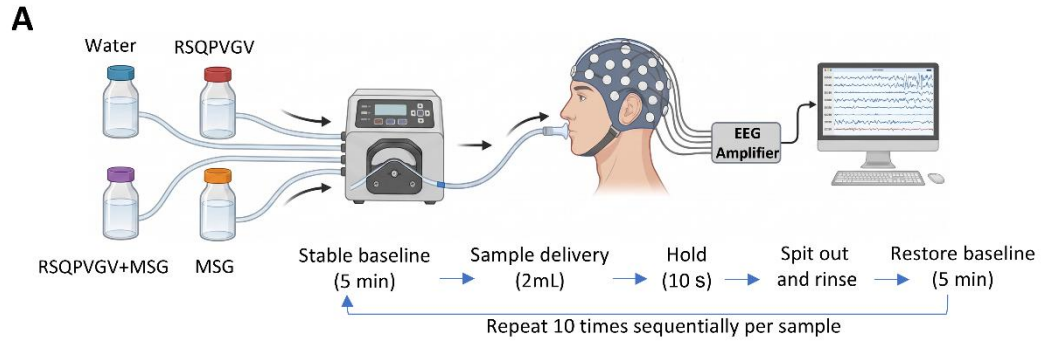
Group	Immobilized molecule	Flowing molecule	Panels
1	CaSR	GSH	C, D
2	CaSR	RSQPVGV	E, F
3	GSH	CaSR-NPS2143	G
4	RSQPVGV	CaSR-NPS2143	H

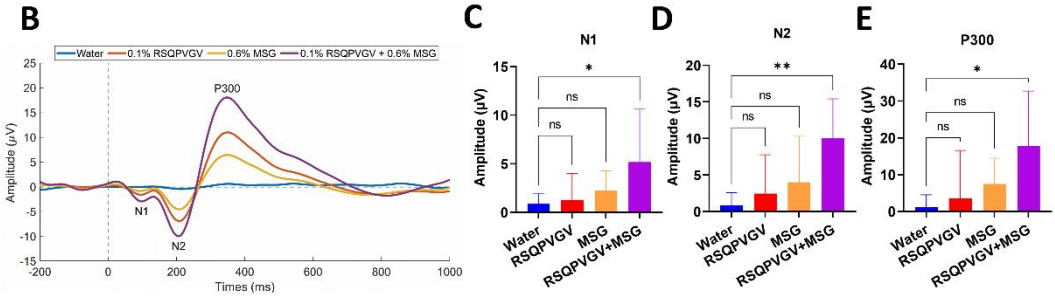


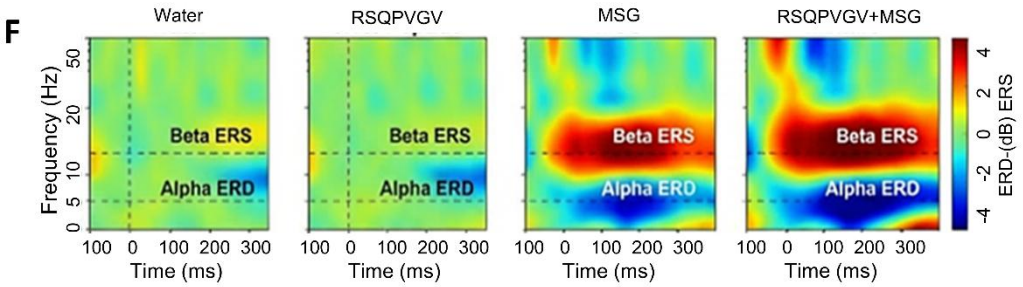

A
B
C
D
E
Sour
Sweet
Bitter
Salty
Umami
Kokumi
MNS
MNS+0.1%GSH
MNS+0.1%RSQPVGV
Taste intensity
Salty
Umami
Kokumi
Richness Value
MNS
MNS+0.1%GSH
MNS+0.1%RSQPVGV

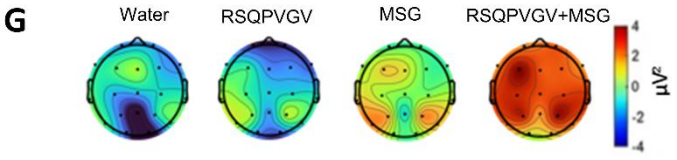

A
B
MNS (1% MSG+0.3% NaCl)
Preference Score
Dilution Ratio of MNS
C
0.1% GSH
Preference Score
DW
0.6MNS
0.6%MSG
0.18%NaCl
0.1mol/L Surcose
Solution
D
0.1% RSQPVGV
Preference Score
Solution
E
0.6% MSG
0.6% MSG + 0.1% GSH
0.6% MSG + 0.1% GSH + 0.005% NPS-2143
Cumulative licks
Time (s)
F
0.6% MSG
0.6% MSG + 0.1% RSQPVGV
0.6% MSG + 0.1% RSQPVGV + 0.005% NPS-2143
Cumulative licks
Time (s)
G
Total licks
MNS
MNS+GSH
MNS+GSH +NPS-2143
H
Total licks
MNS
MNS+GSH
MNS+GSH +NPS-2143

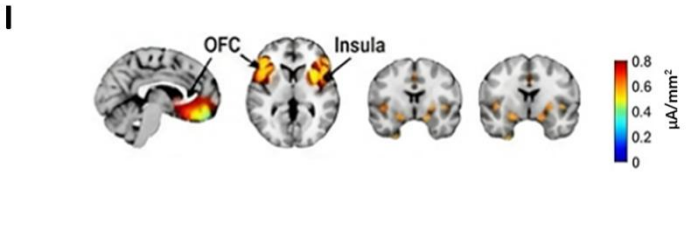

A
Distill Water
0.1%RSQPVGV
0.6%MSG
0.6%MSG+0.1%RSQPVGV
Optical Fiber Signal
24 h water deprivation → randomized presentation →
4 successive rounds → each mouse tested with all 4 solutions
B
10% df/f
10 s
Amplifier & DAQ
CMOS
LED
lens
C
AAV2/9-mCaMKIIα-GCaMP6s-WPRE-pA
Gustatory cortex
D
0.1% RSQPVGV
Lick Burst
ΔF/F0
Time(s)
E
0.6%MSG
Lick Burst
ΔF/F0
Time(s)
F
0.6%MSG
+0.1%RSQPVGV
Lick Burst
ΔF/F0
Time(s)
G
AUC analysis window
Lick Burst
ΔF/F0
Time(s)
H
AUC of ΔF/F0
ns
*
Distill Water
0.1%RSQPVGV
0.6%MSG
0.6%MSG+0.1%RSQPVGV


A
Water
RSQPVGV
RSQPVGV+MSG
MSG
EEG Amplifier
Stable baseline (5 min)
Sample delivery (2mL)
Hold (10 s)
Spit out and rinse
Restore baseline (5 min)
Repeat 10 times sequentially per sample


B
Water
0.1% RSQPVGV
0.6% MSG
0.1% RSQPVGV + 0.6% MSG
P300
N1
N2
Amplitude (μV)
Times (ms)
C
N1
D
N2
E
P300
Amplitude (μV)
Water
RSQPVGV
MSG
RSQPVGV+MSG


F
Water
RSQPVGV
MSG
RSQPVGV+MSG
Frequency (Hz)
Beta ERS
Alpha ERD
Time (ms)
ERD-(dB) ERS


G
Water
RSQPVGV
MSG
RSQPVGV+MSG
μV²
H
β Power (μV²)
Water
RSQPVGV
MSG
RSQPVGV+MSG


I
OFC
Insula
μA/mm²
J
OFC Current Density (μA/mm²)
Water
RSQPVGV
MSG
RSQPVGV+MSG

Supplementary Files

This is a list of supplementary files associated with this preprint. Click to download.

- SupplementaryFiles.docx